2016-09

Characterization and reliability of vertical n-type gallium nitride Schottky contacts

Gardner, Michael L.

Monterey, California: Naval Postgraduate School

NAVAL POSTGRADUATE SCHOOL

MONTEREY, CALIFORNIA

THESIS

CHARACTERIZATION AND RELIABILITY OF VERTICAL N-TYPE GALLIUM NITRIDE SCHOTTKY CONTACTS

by

Michael L. Gardner

September 2016

Thesis Advisor: Todd R. Weatherford
Second Reader: Matthew A. Porter

Approved for public release. Distribution is unlimited.

THIS PAGE INTENTIONALLY LEFT BLANK

REPORT DOCUMENTATION PAGE			*Form Approved OMB No. 0704–0188*

1. AGENCY USE ONLY *(Leave blank)*	**2. REPORT DATE** September 2016	**3. REPORT TYPE AND DATES COVERED** Master's thesis

4. TITLE AND SUBTITLE
CHARACTERIZATION AND RELIABILITY OF VERTICAL N-TYPE GALLIUM NITRIDE SCHOTTKY CONTACTS

5. FUNDING NUMBERS

6. AUTHOR(S) Michael L. Gardner

7. PERFORMING ORGANIZATION NAME(S) AND ADDRESS(ES)
Naval Postgraduate School
Monterey, CA 93943-5000

8. PERFORMING ORGANIZATION REPORT NUMBER

9. SPONSORING /MONITORING AGENCY NAME(S) AND ADDRESS(ES)
N/A

10. SPONSORING / MONITORING AGENCY REPORT NUMBER

11. SUPPLEMENTARY NOTES The views expressed in this thesis are those of the author and do not reflect the official policy or position of the Department of Defense or the U.S. Government. IRB Protocol number ____N/A____.

12a. DISTRIBUTION / AVAILABILITY STATEMENT
Approved for public release. Distribution is unlimited.

12b. DISTRIBUTION CODE

13. ABSTRACT (maximum 200 words)

Silicon- and silicon carbide-based power devices have dominated the power electronics industry. For many emerging high-current and high-power applications, vertical transport gallium nitride (GaN)-based devices are more desirable. In this study, a series of reduced-defect, vertical *n*-type GaN Schottky contacts were fabricated and subjected to high-current density accelerated lifetime tests to understand the physics of contact degradation and compare the reliability of different metallization types and process cleans. Tested Schottky metals included molybdenum, molybdenum-gold, and chromium-gold. Process cleans compared were a piranha etch and a hydrofluoric acid etch. Pre-stress electrical characterization confirmed functioning Schottky contacts and determined device electrical performance parameters. Using a stress-measure-stress system, we obtained results of high-current density accelerated lifetime testing of 170 hours at current densities of 2.3 $kAcm^{-2}$ that showed both catastrophic and non-catastrophic failures across all metallization types and process cleans. While comparative analysis showed that molybdenum was the most reliable, identified experimental testing and non-ideal fabrication issues limited the conclusivity of the results. The identified constraints and initial comparative results serve to inform future Schottky contact structural design and fabrication for future optimized testing

14. SUBJECT TERMS accelerated lifetime testing, Schottky barrier height inhomogeneity, gallium nitride, vertical transport, power electronics, high current density, semiconductor reliability			**15. NUMBER OF PAGES** 101
			16. PRICE CODE
17. SECURITY CLASSIFICATION OF REPORT Unclassified	**18. SECURITY CLASSIFICATION OF THIS PAGE** Unclassified	**19. SECURITY CLASSIFICATION OF ABSTRACT** Unclassified	**20. LIMITATION OF ABSTRACT** UU

NSN 7540–01-280-5500

Standard Form 298 (Rev. 2–89)
Prescribed by ANSI Std. 239–18

THIS PAGE INTENTIONALLY LEFT BLANK

Approved for public release. Distribution is unlimited.

CHARACTERIZATION AND RELIABILITY OF VERTICAL N-TYPE GALLIUM NITRIDE SCHOTTKY CONTACTS

Michael L. Gardner
Major, United States Marine Corps
B.S.E.E., University of Minnesota, 2004
M.S.S.I., National Defense Intelligence College, 2011

Submitted in partial fulfillment of the
requirements for the degree of

MASTER OF SCIENCE IN ELECTRICAL ENGINEERING

from the

NAVAL POSTGRADUATE SCHOOL
September 2016

Approved by: Todd R. Weatherford, Ph.D.
Thesis Advisor

Matthew A. Porter
Second Reader

R. Clark Robertson, Ph.D.
Chair, Department of Electrical Engineering

THIS PAGE INTENTIONALLY LEFT BLANK

ABSTRACT

Silicon- and silicon carbide-based power devices have dominated the power electronics industry. For many emerging high-current and high-power applications, vertical transport gallium nitride (GaN)-based devices are more desirable. In this study, a series of reduced-defect, vertical *n*-type GaN Schottky contacts were fabricated and subjected to high-current density accelerated lifetime tests to understand the physics of contact degradation and compare the reliability of different metallization types and process cleans. Tested Schottky metals included molybdenum, molybdenum-gold, and chromium-gold. Process cleans compared were a piranha etch and a hydrofluoric acid etch. Pre-stress electrical characterization confirmed functioning Schottky contacts and determined device electrical performance parameters. Using a stress-measure-stress system, we obtained results of high-current density accelerated lifetime testing of 170 hours at current densities of 2.3 $kAcm^{-2}$ that showed both catastrophic and non-catastrophic failures across all metallization types and process cleans. While comparative analysis showed that molybdenum was the most reliable, identified experimental testing and non-ideal fabrication issues limited the conclusivity of the results. The identified constraints and initial comparative results serve to inform future Schottky contact structural design and fabrication for future optimized testing.

THIS PAGE INTENTIONALLY LEFT BLANK

TABLE OF CONTENTS

LIST OF FIGURES

LIST OF TABLES

THIS PAGE INTENTIONALLY LEFT BLANK

LIST OF ACRONYMS AND ABBREVIATIONS

BHI	barrier height inhomogeneity
CrAu	chromium gold
C-V	capacitance-voltage
EDS	energy-dispersive X-ray spectroscopy
EECP	equilibrium of electrochemical potential
GaAs	gallium arsenide
GaN	gallium nitride
HEMT	high-electron mobility transistor
HF	hydrofluoric acid
H_2O_2	hydrogen peroxide
HPVE	hydride vapor phase epitaxy
H_2SO_4	sulfuric acid
InP	indium phosphide
ISR	interface specific region
I-V	current-voltage
I-V-T	current-voltage-temperature
LCR	inductance capacitance resistance
MIGS	metal-induced gap states
MFCMU	multi-frequency capacitance measure unit
Mo	molybdenum
MoAu	molybdenum gold
MOCVD	metal-organic chemical vapor deposition
Pd	palladium
Pt	platinum
RF	radio frequency
SBD	Schottky barrier diode
SEM	scanning electron microscopy
SiC	silicon carbide
SMU	source measure unit

THIS PAGE INTENTIONALLY LEFT BLANK

ACKNOWLEDGMENTS

Foremost, I would like to thank my wife, Melissa, with whom I have three wonderful children. Without her endless love, unwavering support, and selfless sacrifices, the time and effort required to produce this thesis would not have been possible. While I spent hundreds of hours conducting research in the lab and studying in the library, she cared for our children and created a loving home for our family. Her strength, passion, and kindness served as my daily inspiration. I owe much, if not all, of my success to her. For all of the aforementioned reasons, and much more, I am forever grateful.

I would also like to thank Dr. Todd Weatherford for allowing me the opportunity to fulfill my intellectual curiosity through conducting this professional scientific research. Through his tutelage and personal mentorship, he instilled in me a renewed passion for semiconductor devices and related technologies that I look forward to pursuing after the Marine Corps.

I would also like to thank Matthew Porter. He spent countless hours working with me and drilling me on semiconductor fundamentals and associated research topics. Without his instructions and dedicated effort, I would have never formed the requisite baseline knowledge to conduct advanced research within the semiconductor field. In addition, he served as a trusted and valuable sounding board for numerous research ideas and related issues. Overall, he drove me to become a true electrical engineer, and I appreciate that.

Lastly, I would like to thank Dr. Sherif Michael, Dr. Gamani Karunasiri, Dr. Dragoslav Grbovic, Dr. Sarath Menon, and the rest of the faculty and staff of the Graduate School of Engineering and Applied Sciences. The renowned faculty and support staff were instrumental to my success at Naval Postgraduate School.

THIS PAGE INTENTIONALLY LEFT BLANK

I. INTRODUCTION

A. BACKGROUND

The United States military continues to field some of the most advanced technologies in the world, from the Joint Strike Fighter to the Zumwalt Class Destroyer to advanced energy weapons systems; however, with advanced technologies, comes demand for increased energy and electrical performance. To mitigate these demands, a need for greater energy efficiency and better performing technologies exists. The military industrial complex, relying heavily on the innovation of the semiconductor and electronic device industries, has easily met these demands over the last few decades. Improved circuit design and the improvement in silicon (Si) processing technology brought about by Moore's law have allowed the electronics and semiconductor industries to continue to increase power device performance. Nevertheless, this continued trajectory of greater energy efficiency and higher performance is leveling-off, mainly due to the physical limits of the most widely used semiconductor materials.

The electronics and semiconductor industries have exploited the material benefits of silicon for several decades. The abundance of silicon, the availability of a high-quality native oxide and the relative ease of fabricating ultra-pure, large diameter Si wafers has enabled rapid advancement in military technologies and consumer electronics; however, material limitations of Si for power electronic applications render it unsuitable for emerging demands in pulsed-load and high power weapons and technologies. To meet these new demands, the power semiconductor industry has turned to wide bandgap semiconductor materials such as gallium nitride (GaN) and silicon carbide (SiC) for future power device applications.

The use of GaN-based power devices is not a new concept. GaN has been focused upon as one of the most anticipated material for power devices [1]. The wide bandgap, high electric breakdown field, high electron mobility and high electron saturation velocity of GaN offer potentially better performance and power efficiency than pure Si or even SiC power devices. Theoretically, GaN devices should operate at higher currents, higher

voltages, and higher power densities, outperforming Si and SiC devices; however, growing low defect density GaN for semiconductor and electronic device fabrication has been cost prohibitive over the years. As such, industry has developed more fiscally feasible lateral GaN power devices on SiC, Si, sapphire and other material substrates. These lateral GaN devices are optimal for radio frequency (RF) applications and have several distinct advantages over Si and SiC; however, lateral GaN devices are not ideal for power applications due to lattice mismatches between the different materials and the innate disadvantages of lateral devices such as lower power density efficiencies. Within the past five years, a few semiconductor foundries have shown the ability to grow reduced-dislocation pure GaN substrates, which was the difficulty in realizing vertical GaN power devices [1].

Of all the GaN power devices, the most fundamental and critical, albeit still not completely understood, is arguably the Schottky barrier diode (SBD). The SBD is a fundamental component in the majority of power electronic devices; specifically, those used in the operation of emerging military electrical weapons and technologies. SBDs are also used in a wide-range of power converters. The comparatively low forward voltage drop and fast switching capability of SBD reduces power losses while increasing system efficiency. In addition, SBDs have a wide range of photovoltaic applications due to low reverse current and significant discharge protection capabilities of SBDs. The theoretical material advantage of GaN over Si and SiC make GaN-based SBDs ideal for future Navy energy efficient and power electronic needs [1].

B. RELATED WORK

The study of GaN for electronic applications has been ongoing for over three decades as material scientists, solid-state physicists and electrical engineers have sought to improve the material quality of GaN and perfect device fabrication techniques for RF and power applications. In 1983, Kahn, Skogman, Schulze, and Gershenzon examined the electrical and material properties of GaN [2], where it is shown that GaN, a direct bandgap semiconductor, has a higher electron mobility and higher electric breakdown

voltage than Si and SiC. These results demonstrated the significant power application advantages that a GaN based power device has over Si or SiC based power devices.

Due to the importance of the Schottky barrier to the performance of a Schottky contact, numerous studies have examined the characteristics and stability of the Schottky barrier of GaN Schottky contacts. Schmitz, Ping, Khan, Chen, Yang, and Adesida focused on investigating and determining the Schottky barrier height of palladium (Pd), platinum (Pt), chromium (Cr), titanium (Ti), gold (Au), and nickel (Ni) on n-GaN material [3]. Relying on the widely accepted thermionic-emission-diffusion theory, as proposed by Crowell and Sze in [4], these studies used current-voltage-temperature (I-V-T), capacitance-voltage (C-V), and photoemission spectroscopy measurement techniques to determine the Schottky barrier height and other Schottky contact characteristics. These methods were also used by Wang, Nathan, Lim, Kahn and Chen to characterize lateral Pt/GaN and Pd/GaN Schottky contacts [5]. The deterministic nature of these methods led to the ability to characterize the long-term reliability of Schottky contacts by the change over time of the ideality factor, leakage current, Schottky barrier height, and series resistance, which was used by Zhang to study the reliability of SiC Schottky contacts [6]. More recently in 2015, Yoshimoto, Okada, Mitshuashi, Ishizuka, and Ueno demonstrated the long-term reliability of vertical metal-GaN Schottky barrier diodes through their analysis of the degradation of the leakage current and forward voltage over time [7]. While these studies investigated the reliability and long-term performance of GaN Schottky contacts, literature and definitive understanding of the degradation mechanisms and mean-time-to-failure of GaN Schottky contacts for power applications is still lacking.

C. PROBLEM STATEMENT AND RESEARCH OBJECTIVES

A reliable metal for Schottky contacts on GaN for high power applications has not been demonstrated in past research. Historical reliability studies on GaN Schottky contacts focus primarily on lateral GaN high electron mobility transistors (HEMTs) and associated gate Schottky contact degradation. While useful, these studies are not directly applicable to the high current density operating conditions found in power applications. Minimal information exists that provides useful and applicable insight on potential

degradation mechanisms of vertical GaN Schottky contacts for power applications. This work attempts to provide clarity to this problem by conducting a high current density accelerated lifetime test of various reduced dislocation density GaN Schottky contacts grown on newly available high quality vertical GaN substrates. Subsequent analysis focuses on comparative studies among the Schottky metals and associated fabrication processes.

Our research effort includes the fabrication of vertical *n*-type GaN Schottky contacts at Sandia National Laboratories using vertical GaN substrates provided by Avogy Inc. with contact metals of Pt, Pd, Mo, and Cr. Fabrication is followed by the characterization, testing, and analysis of the metal-semiconductor (MS) interface of GaN Schottky contacts. Current-voltage (I-V), current-voltage-temperature (I-V-T) and capacitance-voltage (C-V) characterizations are performed to analyze device performance and material properties. High current density accelerated lifetime tests and electrical and optical spectroscopy are used to determine probable degradation mechanisms and to compare metal contacts.

D. THESIS ORGANIZATION

The basic physics of Schottky contacts and associated interface models, current transport processes and barrier height inhomogeneity, along with a discussion of Schottky contact reliability, are examined in Chapter II. In Chapter III, the experimental methodology, setups and designs utilized within this study are described. The experimental results are discussed and analysis and proposed degradation mechanisms are presented in Chapter IV. Finally, study conclusions and future recommendations are provided in Chapter V.

II. BACKGROUND AND THEORY

A brief review of the fundamental physics of metal-semiconductor Schottky contacts is presented in this chapter. The review highlights the important Schottky contact parameters, the current transport mechanism associated with wide-bandgap semiconductor based Schottky contacts, and the progression of physical models of Schottky barriers. In addition, a brief overview on the topic of the reliability of high power Schottky contacts is presented.

A. FUNDAMENTALS OF SCHOTTKY CONTACTS

To better understand the relevant physics and associated parameters of Schottky contacts, a review of the fundamentals of Schottky contact formation and carrier transport are presented in this section. Discussed are the types of MS junctions, the Schottky contact charge depletion region, the relevant current transport process and the associated Schottky contact electrical characterization methods.

1. Metal-Semiconductor Junctions

When a metal comes into close contact with a semiconductor material, a MS junction is formed. The resultant MS junction is classified as either non-rectifying, forming an ohmic contact, or rectifying, forming what is known as a Schottky contact. Generally, the difference between the two is observed through the differences in the DC current-voltage (I-V) relationship of a two-terminal device formed by the contact in question and a second ohmic contact. Ohmic contacts possess linear, resistive I-V relationships, while Schottky contacts possess non-linear, rectifying I-V relationships, as comparatively shown in Figure 1.

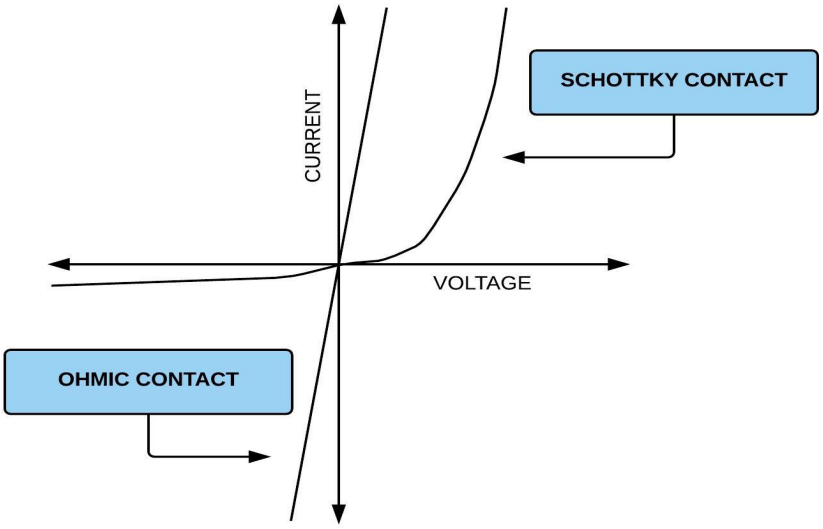

Figure 1. Diagram of Current - Voltage (I-V) Relationship of MS Junctions.

In either case, a carrier-transport barrier is established between the metal and the semiconductor at the interface and is characterized by the barrier height ϕ_B [8, 9]. The carrier-transport barrier, called Schottky barrier, is the critical current transport parameter of MS junctions. For *n*-type MS junctions, the Schottky barrier height ϕ_{Bn} is defined as the difference between the bottom energy level of the conduction band E_c at the MS junction and the Fermi level of the metal E_{Fm} [10]. A simple view of the energy band diagram of an *n*-type MS junction with corresponding barrier height annotated is shown in Figure 2.

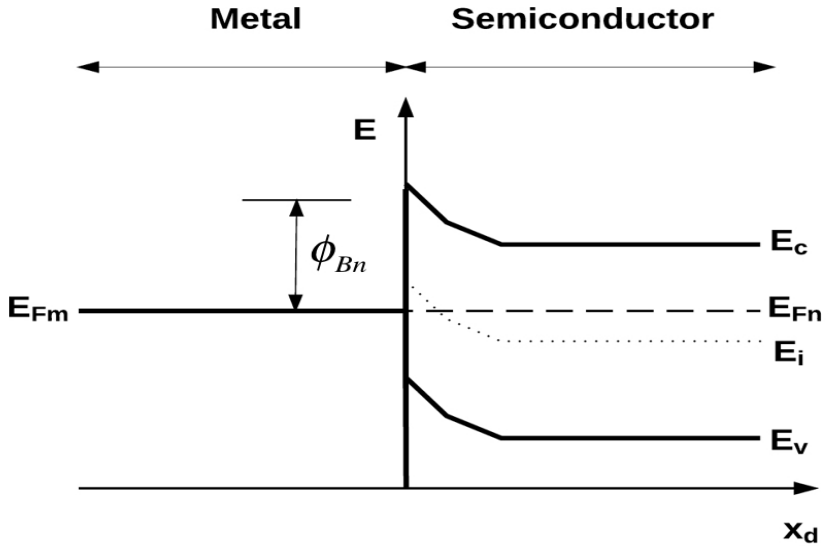

Figure 2. Ideal Energy Band Diagram of *n*-type MS Junction.

2. Schottky Contact Depletion Layer

The Schottky contact depletion layer is akin to a one sided abrupt *p*+-*n* junction in that the depletion layer exists effectively only within the moderately doped semiconductor material [10]. As a result, using the abrupt depletion approximation and associated Schottky contact based boundary conditions for Poisson's equation, the depletion width W_D of the Schottky contact can be shown to be given by [10]

$$W_D = \sqrt{\frac{2\varepsilon_o\varepsilon_r}{qN_D}\left(\psi_{bi} - V_a - \frac{kT}{q}\right)} \tag{1}$$

where ε_o is the vacuum permittivity, ε_r is the relative static permittivity of the semiconductor material, q is the charge of an electron, N_D is the doping concentration of the semiconductor, ψ_{bi} is the built-in potential of the Schottky contact, V_a is the applied bias voltage, k is Boltzmann's constant and T is temperature in Kelvin.

Under the depletion approximation, the only charges present in the depletion region are ionized donors. The total space charge Q_{sc} is equal to the product of the ionized donors and the depletion width and is given by [10]

$$Q_{sc} = qN_D W_D \,. \tag{2}$$

Capacitance being the change of charge with voltage, the MS Schottky contact junction capacitance C_D can be shown to be a function of voltage. From Equation (2),

$$C_D = \frac{dQ_{sc}}{dV_a} = \sqrt{\frac{q\varepsilon_o \varepsilon_r N_D}{2\left(\psi_{bi} - V_a - \frac{kT}{q}\right)}}. \tag{3}$$

Assuming a non-degenerate doping profile within the depletion layer, we use a measurement of capacitance versus applied voltage to measure doping level of the semiconductor by plotting $1/C^2$ versus applied voltage. The result should be a straight line, as shown in Figure 3, and solving Equation (3) for N_D, we see that the slope of the line is inversely proportional to N_D and is given by

$$N_D = \frac{2}{q\varepsilon_o \varepsilon_r}\left(\frac{1}{slope}\right). \tag{4}$$

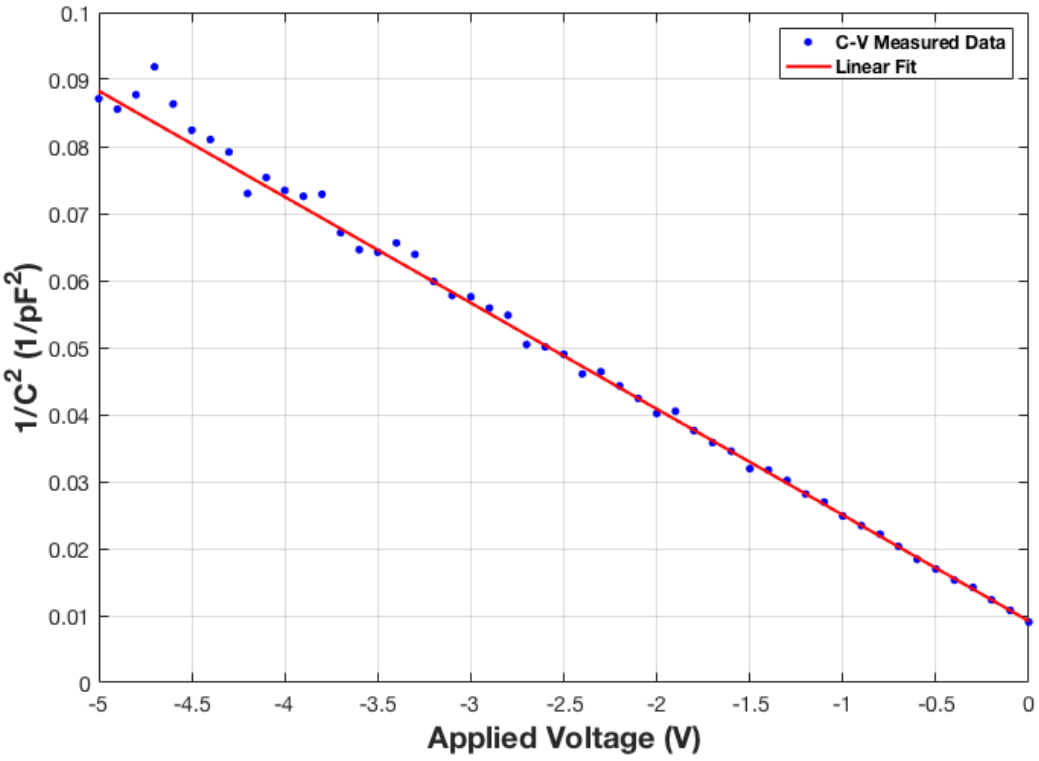

Figure 3. $1/C^2$ versus Applied Voltage for a Schottky Contact.

3. GaN Schottky Contact Current Transport Process

Schottky contacts are majority carrier devices. There are five primary distinct current transport mechanisms as shown in Figure 4: (1) thermionic emission of carriers across the Schottky barrier, (2) quantum-mechanical tunneling through the Schottky barrier, (3) recombination of electrons and holes in the depletion layer, (4) diffusion of carriers from the semiconductor into the metal, and (5) minority carrier injection [10].

The net current through the junction is the summation of the current contribution from each carrier transport mechanism; however, typically the net current is limited by only one of the mechanisms [8]-[11]. For high mobility *n*-type Schottky contacts like Si, gallium arsenide (GaAs), and GaN, thermionic emission is the dominant transport mechanism [10].

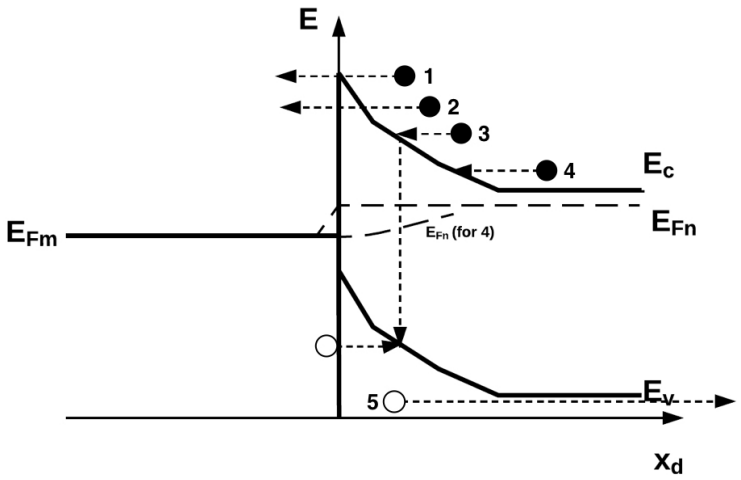

Figure 4. Five Current Transport Processes for *n*-type Schottky Contacts. Adapted from [10].

Thermionic emission is a ballistic transport process. For Schottky contacts, electrons traveling from the metal to the semiconductor that have a higher kinetic energy than the energy barrier presented by the Schottky barrier flow across the MS junction. Conversely, electrons traveling from the semiconductor to the metal that have a higher kinetic energy than the built-in potential ψ_{bi} flow across the MS junction. As a result, the total net current J_n is the sum of the flux of carriers over the Schottky barrier from the metal to semiconductor J_{M-S} and the flux of carriers over ψ_{bi} from the semiconductor to metal J_{S-M} and is given by

$$J_n = J_{M-S} + J_{S-M}. \tag{5}$$

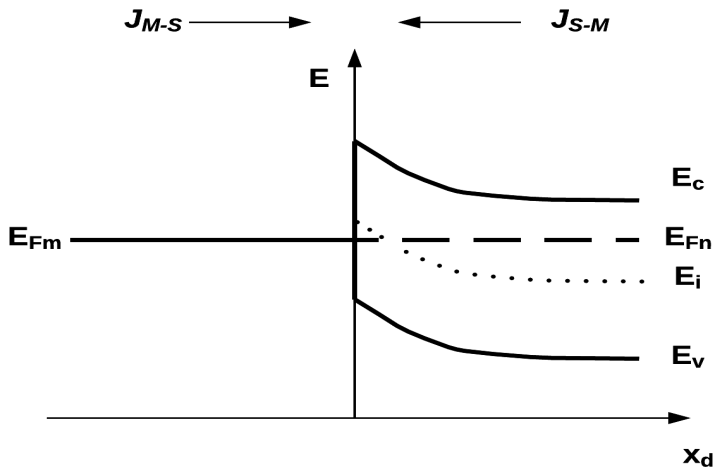

Figure 5. Current Flow Across Schottky Contact.

The resulting thermionic-emission theory net current density J_n is quantitatively described by [10]

$$J_n = \left[A^* T^2 \exp\left(\frac{-q\phi_{Bn}}{kT} \right) \right] \left[\exp\left(\frac{qV_a}{\eta kT} \right) - 1 \right] \tag{6}$$

where ϕ_{Bn} is the Schottky barrier height, η is the ideality factor and A^* is the effective Richardson constant given by

$$A^* = \frac{4\pi q m^* k^2}{h^3}, \tag{7}$$

m^* is the effective mass of an electron for a given material, and h is Plank's constant.

a. Current-Voltage Relationship

A typical theoretical and experimental I-V relationship for an *n*-type GaN Schottky contact is shown in Figure 6. Noting the deviation of the experimental from the theoretical values, three distinct regions appear, as annotated on Figure 6. Region I is where non-thermionic-emission transport processes and non-ideal factors such as

tunneling or recombination due to imperfections of the MS interface that greatly affect the net current occur, typically resulting in higher than expected current levels. The effects of series resistance, which limits the current, dominates region III. Region II is the pure thermionic-emission region where the Schottky barrier height controls the net current.

From Equation (6) and the experimental values within Region II, the values of ϕ_{Bn}, saturation current J_o, and η for the Schottky contact can be determined. Applying Equation (6) to the semi-logarithmic region II produces a linear fit as given by

$$\ln(J_n) = \ln(J_o) + \frac{q}{\eta kT} V_a \tag{8}$$

where J_o is the first part of Equation (6) and is given by

$$J_o = A^* T^2 \exp\left(\frac{-q\phi_{Bn}}{kT} \right). \tag{9}$$

From the linear fit, J_o is the *y*-intercept and η is determined from the slope. Knowing J_o, we can determine barrier height by solving Equation (9) for ϕ_{Bn}; i.e.,

$$\phi_{Bn} = \frac{kT}{q} \ln\left(\frac{A^* T^2}{J_o} \right). \tag{10}$$

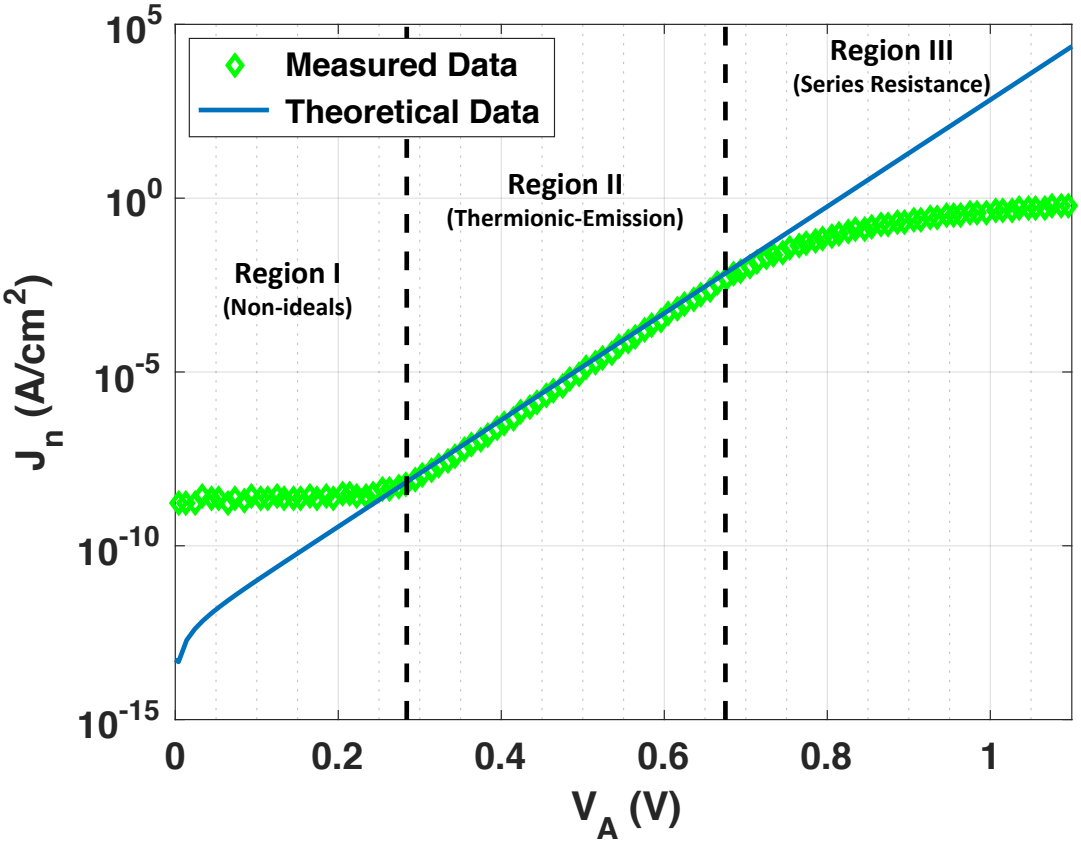

Figure 6. Theoretical and Experimental Semi-Logarithmic I-V Plot for an *n*-type GaN Schottky Contact.

b. Current-Voltage-Temperature Relationship

An accurate determination of ϕ_{Bn} from the thermionic emission current-voltage relationship, given in Equation (10), is dependent upon knowledge of the Richardson coefficient A^*; however, the value of A^* is extremely contact specific and is dependent upon a variety of factors that include annealing temperatures, fabrication methods, metallization process and thickness, and surface cleaning [12]. Although research has shown that even magnitudes of error in A^* produces an error of less than kT/q in the value of the Schottky barrier height, leveraging the temperature dependency of the current-voltage relationship provides for a more accurate method of determining ϕ_{Bn} while also independently determining the value of A^* from experimental data for an individual Schottky contact.

Measuring the current-voltage relationship across a range of temperatures near room temperature and determining J_o for each corresponding temperature enables calculation of the ϕ_{Bn}, η, and A^*. This method is called the activation-energy method and uses what is known as a Richardson plot, a plot of the natural logarithm of the derived J_o values over temperature squared (i.e., J_o/T^2) versus q/kT to calculate ϕ_{Bn} and A^*. A typical Richardson plot for an *n*-type GaN Schottky contact is shown in Figure 7.

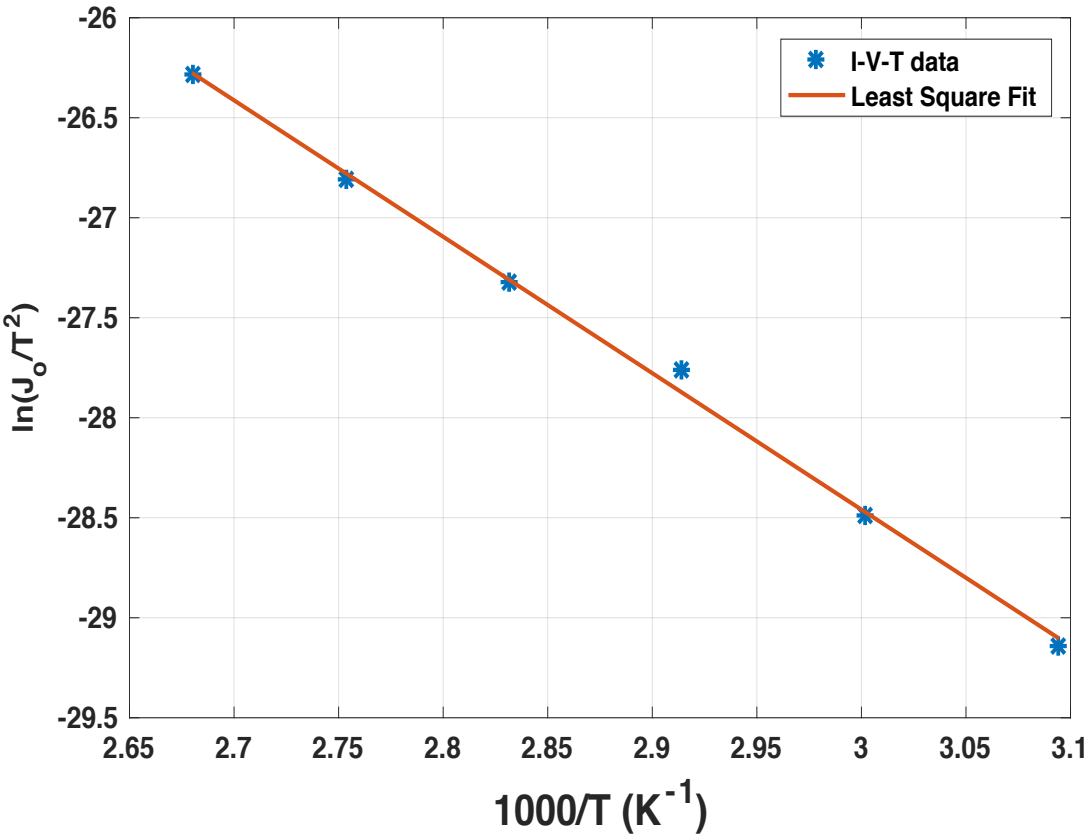

Figure 7. Typical Richardson Plot for a *n*-type GaN Schottky Contact.

Taking the natural logarithm of Equation (9) demonstrates that a least-squares fit to a Richardson plot can be used to extract the barrier height and Richardson coefficient:

$$\ln\left(\frac{J_o}{T^2}\right)=\ln\left(A^*\right)-\frac{q\phi_{Bn}}{kT}. \tag{11}$$

The value of A^* and the value of ϕ_{Bn} are derived from the *y*-intercept and slope, respectively, of the least-squares fit of a Richardson plot for a given Schottky contact.

B. SCHOTTKY BARRIER FORMATION AND MODELS

The SB is critical to the Schottky contact current transport processes and the resulting electrical performance. There exist several methods to determine the Schottky barrier height of a Schottky contact from experimental measurements; however, predicting the magnitude of the Schottky barrier based upon individual bulk metal and semiconductor material proprieties has been challenging to the scientific community. The Schottky-Mott model, considered the model for ideal MS interfaces, states that the difference between the metal work function ϕ_M and the semiconductor electron affinity χ equals the Schottky barrier height ϕ_B:

$$\phi_B = \phi_M - \chi \,. \tag{12}$$

Experimentally measured values of ϕ_B do not correspond directly to the Schottky-Mott model [12]. The deviation from the Schottky-Mott model can be attributed the faulty underlying fundamental assumptions of the Schottky-Mott model. The Schottky-Mott model attributes the properties of the bulk semiconductor to the MS interface. This enables correct visualization of the band bending in Schottky contact energy diagrams; however, the Schottky-Mott model explicitly discounts any potential atomic-level interactions or conditions at the MS interface and the resultant effect on the Schottky barrier height.

1. Interface Specific Region Models

A more accurate prediction of the ϕ_B and understanding of the underlying physics of the MS interface are achieved through models that focus upon the atomic structure of the interface between the metal and the semiconductor, as depicted in Figure 8.

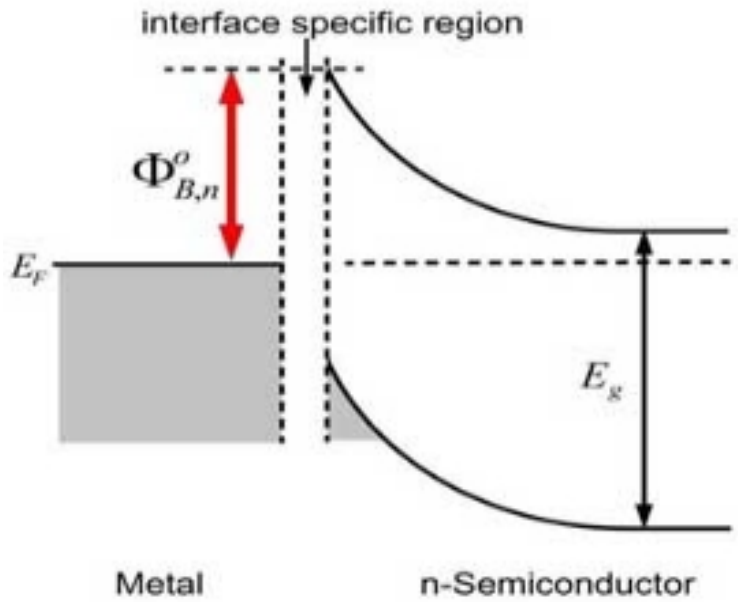

Figure 8. ISR Energy Band Diagram of *n*-type Schottky Contact. Source: [13].

Collectively, these models are categorized as interface specific region (ISR) models and address the emerging understanding of the complex nature of the atomic contact created at the metal semiconductor interface within Schottky contacts. Several models exist for the ISR: the Bardeen model, the Metal-Induced Gap States (MIGS) model, and the modern theoretical Equilibrium of Electrochemical Potential (EECP) model. The early models, Bardeen and MIGS, focused extensively on the notion of Fermi-level pinning, the experimentally observed phenomenon where the Schottky contact's Fermi-level was, to a degree, pinned at an energy-level irrespective of the metal's work function [4, 14, 15]. The Bardeen model explained Fermi-level pinning through the existence of a dielectric interfacial layer and semiconductor surface states while the MIGS model leveraged the idea of existing gap states between the metal and semiconductor material at the interface. While the Bardeen model and the MIGS model facilitated quantitative analysis of the Schottky barrier, these models fall short in predicting the actual physics and atomic interaction at the ISR.

Tung proposed an alternative ISR model, called the EECP model [16]. This modern ISR model for Schottky barrier formation is based upon the natural chemical bonding between metal and semiconductor atoms occurring at the interface; therefore,

Fermi-level pinning is due to the polarization of the interfacial chemical bonds as opposed to surface states or the existence of MIGS. The EECP model still predicts a linear correlation between Fermi-level pinning and the metal workfunction for quantifying ϕ_{Bn}, given by [16]

$$\phi_{Bn} = \gamma_B(\phi_m - \chi) + (1-\gamma_B)\frac{E_g}{2} \tag{13}$$

where the EECP dependent variable γ_B is

$$\gamma_B = 1 - \frac{e^2 d_{MS} N_B}{\varepsilon^{it}(E_g + \kappa)} \tag{14}$$

and d_{MS} is the bond length between the metal and semiconductor atoms at the MS interface, as shown in Figure 9, N_B is the density of chemical bonds across the MS interface, κ is the sum of all hoping interactions, and ε^{it} is the dielectric constant of the interface.

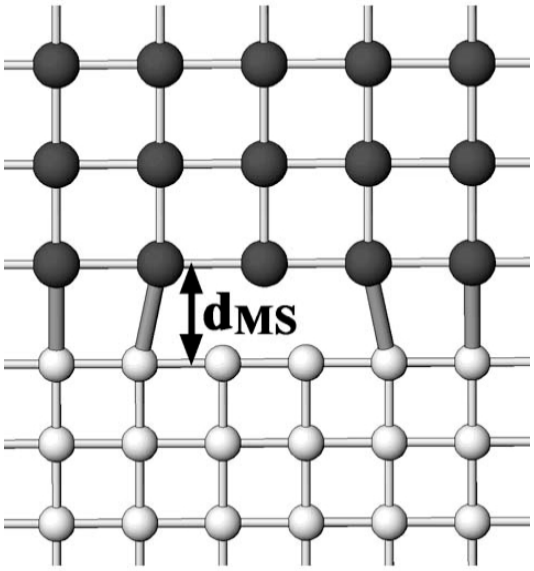

Figure 9. Metal-Semiconductor Interface According to EECP Model.
Source: [16].

More significantly, according to the EECP model, a morphological or chemical change in the bonds across the MS interface correlate to a direct change in the Schottky barrier height. This is important in the investigation of Schottky contact reliability. A measured change in the barrier height of a Schottky contact under stress is indicative of a change in the interface bond structure.

2. Inhomogeneous Schottky Barrier Height

Tung's EECP model goes beyond predicting the Schottky barrier height by providing insight into the inhomogeneous nature of Schottky contacts. If chemical bonding directly affects, or at least is critical to, the Schottky barrier, then intuitively EECP predicts that defects or crystalline mismatches or differences in crystalline orientation at the ISR result in local variation of the Schottky barrier height across the entirety of the Schottky contact, as visualized in Figure 10.

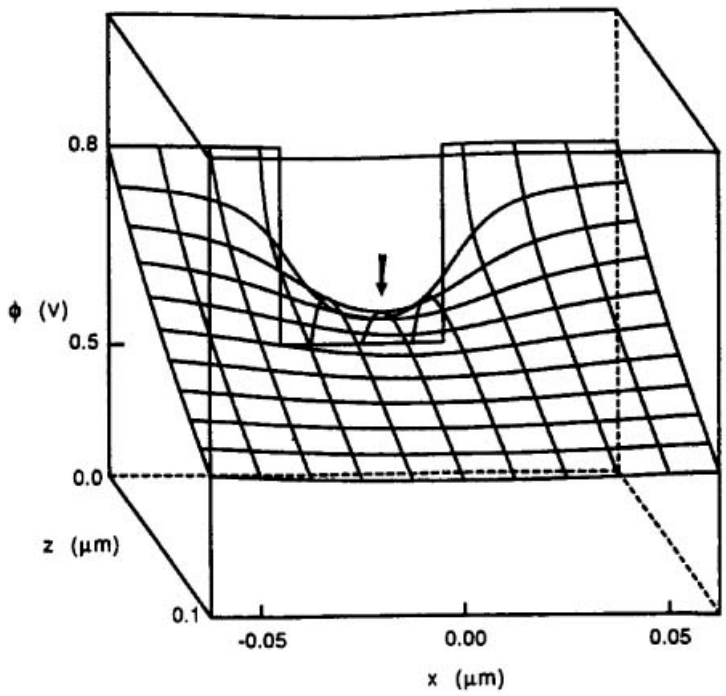

Figure 10. Three-Dimensional View of the Local Variation of the Barrier Height of a Schottky Contact. Source: [12].

A recent study by Balsano, Durcan, Matsubayashi, Narasimham, and LaBella on Schottky barrier height using ballistic electron emission microscopy confirmed this local variation of the Schottky barrier height across the Schottky contact [17]. Holding to the idea of inhomogeneous Schottky barriers, Tung found that experimentally measured values of ϕ_{Bn} reflect the average of the distribution of the true Schottky barrier height, not the true Schottky barrier height of a Schottky contact [12].

a. Effects of Schottky Barrier Inhomogeneity on Current Transport Processes

In the presence of inhomogeneity, current transport equations based upon a uniform Schottky barrier do not accurately describe the actual current flow. Initial attempts to quantify current transport of inhomogeneous Schottky contacts focused on parallel conduction or, more simply, summing the individual currents across each distinct Schottky barrier height region [15]. Similar to historical Schottky contact models, the parallel conduction model ignored the effects of adjacent regions of differing Schottky barrier heights on each other and the resultant net current. Tung provided a mathematically intensive analysis of the collective effects of varying Schottky barrier height regions on the total net current I_{tot} [18]

$$I_{tot} = A^{**} A T^2 \exp\left[-\frac{q\phi'}{k\left(T + T_o'\right)}\right]\left[\exp\left(\frac{qV_a}{k\left(T + T_o'\right)}\right) - 1\right] \tag{15}$$

where A^{**} is the apparent Richardson constant given by

$$A^{**} = A^* f(\beta, V_{bb}), \tag{16}$$

T_o' is a constant given by

$$T_o' = \frac{q\xi\kappa V_{b0}^{\xi-1}}{k} \tag{17}$$

and ϕ' is the apparent Schottky barrier height given by

$$\phi^{'} = \phi_{Bn} + \xi\kappa V_{b0}^{\xi-1} \ln\left(\frac{N_C}{N_D}\right). \tag{18}$$

The parameters ξ, κ, and $f(\beta, V_{bb})$ are topography specific as seen in Table 1.

Table 1. Parameters for Current Transport of Area Specific Inhomogeneous Schottky Contacts. Source: [18].

Parameter	Patch	Strip
ξ	2/3	1/2
κ	$\frac{\sigma_1^2}{2\eta^{\frac{2}{3}}}$	$\frac{\sigma_2^2}{2\eta^{\frac{1}{2}}}$
$f(\beta, V_{bb})$	$\frac{8c_1\sigma_1^2\pi\eta^{\frac{1}{3}}}{9V_{bb}^{\frac{1}{3}}}$	$\frac{c_2\pi\sigma_2^{\frac{3}{2}}\sqrt{\beta}\eta^{\frac{1}{8}}L_{strip}}{1.46V_{bb}^{\frac{1}{8}}}$

A significant issue with barrier height inhomogeneity is that it promotes interdependency in carrier transport across the Schottky contact interface. As a result, a phenomenon called current crowding—a condition where a large numbers of carriers are funneled into a relatively small region—occurs [18]. The existence of current crowding in Schottky contacts has the potential to limit current transport through increasing the series resistance. This is especially concerning for power devices where high series resistance drives power loss and higher device temperatures. While the total effect of current crowding is still under investigation, the existence of non-uniform carrier flow across the Schottky contact area possesses significant device performance concerns.

b. Experimental Characterization of Schottky Barrier Height Inhomogeneity

A limitation of Tung's predictive model is the reliance upon requiring knowledge of the topographical nature of the Schottky barrier height inhomogeneity. This is a significant problem when dealing with novel materials where research and data are scarce. A better means is to accept the existence of inhomogeneity and characterize the degree of inhomogeneity. Characterizing the degree of inhomogeneity is especially useful for comparative purposes. A few proposed methods of experimentally characterizing inhomogeneity exist [19]–[21].

An early effort by Werner and Guttler proposed an analytical method to characterize inhomogeneity through relating the true zero-bias Schottky barrier height ϕ_{Bo} as a function of the experimentally measured, or apparent, Schottky barrier height ϕ_{ap} given by [19]

$$\phi_{ap} = \phi_{Bo} - \frac{q\sigma_{so}^2}{2kT} \tag{19}$$

where σ_{so} is the zero-bias standard deviation of the barrier height distribution, a parameter used to characterize inhomogeneity. Furthermore, according to Werner and Guttler, barrier height inhomogeneity is confirmed if the ideality factor η is temperature dependent and can be expressed as

$$\frac{1}{\eta} - 1 = -\rho_1 - \frac{q\rho_2}{2kT} \tag{20}$$

where ρ_1 is the voltage coefficient of the mean Schottky barrier height and ρ_2 is the voltage coefficient of σ_{so}. A plot of (19) and (20) versus the inverse of temperature should give a straight line where the *y*-intercept and slope for (19) and (20) determine ϕ_{Bo}, σ_{so} and ρ_1, ρ_2, respectively. Kumar, Arafin, Amann, and Singh successfully used the Werner and Guttler method to characterize Schottky barrier inhomogeneity of *n*-type Pt/GaN Schottky contacts [22]. Their resultant plots are shown in Figure 11.

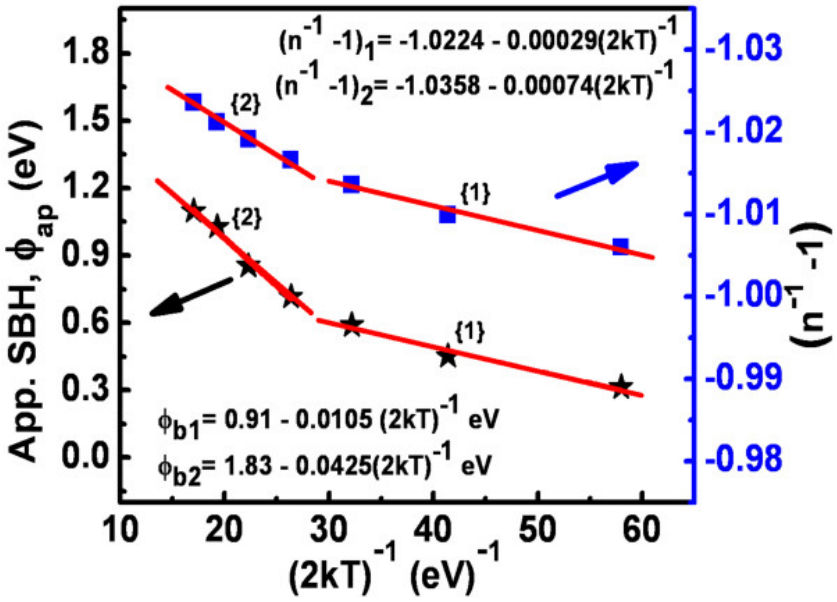

Figure 11. Inhomogeneous Pt/GaN Schottky Contact Apparent Schottky Barrier Height and Temperature Dependent Ideality Factor. Source: [22].

Relying upon the temperature dependence anomaly, referred to as the T_o anomaly and first proposed Padovani and Sumner in [21], another approach incorporating Tung's model of Schottky barrier used to determine the inhomogeneity parameters was discussed in [20]. While limitations of the T_o-based approach are discussed in [20], the T_o-based approach addresses the weakness of the aforementioned Werner and Guttler method.

The T_o anomaly is derived directly from the discovery that Schottky contacts that exhibit inhomogeneity are experimentally found to have an ideality factor directly related to temperature, as given by

$$\eta = 1 + \frac{T_o}{T} \tag{21}$$

where T_o is function of the Schottky barrier inhomogeneity parameters, as expressed by

$$T_o = \left(\frac{\sigma^2}{3n\beta_1} \right) \frac{q}{k}, \tag{22}$$

σ is the patch spread parameter, n is the doping density parameter, and β_1 is a function of the Schottky contact built-in voltage given by

$$\beta_1 = \left(\frac{V_{bi}}{n} \right)^{\frac{1}{3}}. \tag{23}$$

Experimentally determining η for various temperatures, we can readily calculate σ using Equations (21) – (23) as the value of σ is the only unknown. The other values are a function of either measured parameters, such as V_{bi}, or material dependent constants, such as n. To calculate σ, we use Equation (21) to linearly fit a plot of η versus $1/T$, and the slope of that fit is T_o. The inhomogeneity parameter σ is then calculated using Equation (22).

The other key characterizing inhomogeneity parameter, the total density of inhomogeneous patches C_1, is derived from a modified Richardson's plot derived from a modification of Equation (11) through incorporating Tung's effective Schottky barrier height area, which can be expressed as

$$\ln\left(\frac{J_o}{T^2} \right) = \ln\left(fA^* \right) - \frac{q\phi_{app}}{\eta kT} \tag{24}$$

where *f* is the Schottky barrier height inhomogeneity effective area parameter given by

$$f = \frac{8C_1\pi\sigma^2}{9\beta_1}. \tag{25}$$

The parameter C_1 is now determined by taking the difference between the *y*-intercept values of the Richardson's plot and modified Richardson's plot linear fits, Equation (11) and Equation (24), respectively. The difference is equal to the natural logarithm of *f*. Knowing the value of *f*, we can use Equation (25) to calculate C_1. While not predictive in nature, this method can be easily executed on any Schottky contact through I-V-T measurements to determine the Schottky barrier inhomogeneous C_1 and σ parameters for comparative purposes [20].

C. RELIABILITY OF GALLIUM NITRIDE SCHOTTKY CONTACTS

The essence of useful and effective Schottky contacts for power applications is the ability to perform consistently under high power loads over extended periods. In order to engineer such devices, potential degradation mechanisms need to be understood.

1. Historical Reliability and Failure Analysis of Schottky Contacts

Reliability and failure analysis of Si-based power devices studies illustrated that metal diffusion and movement of material away from the MS interface increased the internal resistance of the device, leading to thermal runaway and, ultimately, device failure [23]–[25]. Brandt, Krozer, Schubler, Bock, and Hartnagel showed that GaAs Schottky diodes operated under high current density stress were prone to catastrophic failure due to the creation of hot filaments generated inside the material that destroyed the MS interface through overstress caused by excessively high junction temperatures [26]. In most cases, the specific degradation mechanism was highly dependent upon the metallization [27].

The emergence of SiC with higher breakdown electric field and better thermal conductivity promised greater potential for increased power efficiencies while, theoretically, having fewer degradation issues. This led to increased failure analysis studies of SiC Schottky barrier diodes, which that showed that in response to high current densities, joule heating driven diffusion and unwanted material reactions lead to voiding, highly resistive regions and shorted junctions [28]. In addition to internal device morphological changes, Downey, Flemish, Liu, Clark, and Mohney showed that the unwanted metal-semiconductor reactions manifested in surface contact deformation, as seen in Figure 12 [27]. Many of these degradation concerns and problems for SiC-based power devices were resolved through advancement in fabrication techniques, changes to design topologies, and through the use of reduced dislocation density and minimally strained SiC substrates.

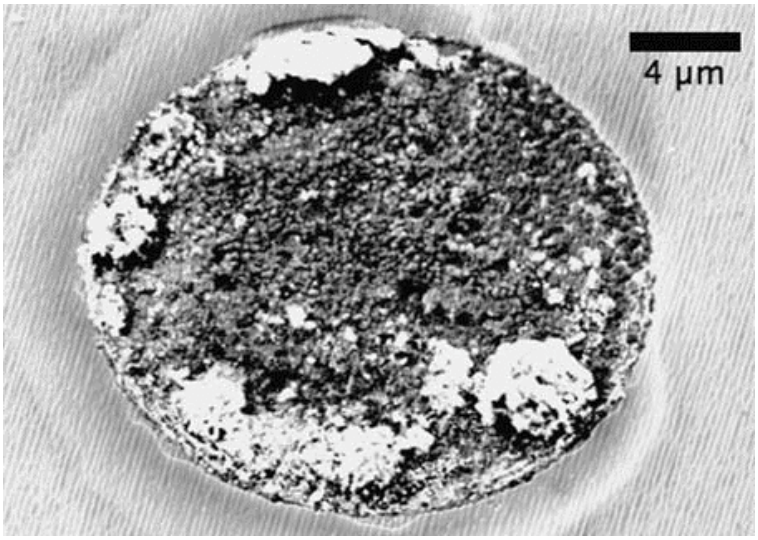

Figure 12. SEM Micrograph of Degraded SiC MS Junction. Source: [27].

Until recently, GaN semiconductor devices were all lateral design, largely due to the practice of growing GaN drift layers on sapphire, Si or SiC substrates. GaN lateral devices do not possess the high current conduction capabilities of vertical GaN devices. As a result, very few reliability and failure analysis studies of vertical *n*-type GaN Schottky contacts exist. The majority of the reliability and failure analysis studies of GaN Schottky contacts are related to the Schottky gates of GaN high electron mobility transistors (HEMT). A comprehensive review of these studies by Zanoni, Meneghini, Chini, Marcon, and Meneghesso noted that the reliability and failure mechanisms of GaN are likely to differ from historical Si and GaAs power devices, specifically, failures due to electrochemical degradation, inverse piezoelectric effect, and metal-metal and metal-semiconductor interdiffusion [29]. While possible solutions were proposed for lateral GaN-based devices, long-term reliability of vertical GaN Schottky contacts when operated under high current density remains an issue [29].

2. Reliability Testing—Accelerated Lifetime Stress Test

Accelerated lifetime stress tests are the most common type of failure analysis and reliability testing for power electronics devices. The goal of accelerated lifetime tests is to expose devices to higher than normal bias or environmental conditions that stress the device to a point of failure or degradation. Analyzing the results from these tests allows

for predicting device failures, identifying degradation mechanisms, and determining device lifetime performance.

For the purposes of this research, a high current density accelerated lifetime test is used, where a constant DC current bias, at a level far greater than normal operating level, is applied for a long period time. This type of test was successfully used by Zhang to identify catastrophic and, more importantly, non-catastrophic failures of SiC Schottky contacts [6]. Catastrophic failures are easy to identify through post-stress analysis, exhibit no rectifying capability and are known to show significant morphological changes [30]. Zhang showed that by tracking SiC Schottky contact parameters, such as ideality factor, reverse leakage, forward voltage, and Schottky barrier height, over the length of the test, one can identify non-catastrophic failures and associated degradation [6]. To accomplish this a modified high current density accelerated lifetime test, conducting periodic current-voltage sweeps to measure changes in the Schottky contact electrical characteristic, is required. Implementation of a stress-measure-stress high current density accelerated lifetime test increases the amount of data, including both catastrophic and non-catastrophic failed device data, and benefit the failure and reliability analysis of the vertical *n*-type GaN Schottky contacts. Similar work has been done on GaN and GaAs HEMTs [31]. The in-situ data provided insight into the timeliness of device degradation and fostered predictive degradation modeling.

III. EXPERIMENTAL METHODOLOGY

To achieve the research objectives, a three-phase experimental method was executed. In the first phase, electrical characterization tests of the GaN-based Schottky contacts were conducted to determine baseline device and material parameters. The second phase consisted of the accelerated lifetime test that employed a stress-measure-stress system. In the third phase, post-stress test device characterization was done to determine changes in device and material parameters. Herein, each phase and associated test systems are described.

A. GALLIUM NITRIDE SCHOTTKY CONTACT DESIGN AND FABRICATION

A series of vertical *n*-type GaN Schottky contacts were fabricated for testing in this experiment. Deposition of *n*-type GaN Schottky on two-inch quasi-bulk hydride vapor phase epitaxy (HPVE) GaN-wafers purchased from Sumitomo Electric Semiconductor Materials was carried out at Sandia National Laboratories. The GaN drift layer was grown via metal-organic chemical vapor deposition (MOCVD). A listing of relevant bulk and drift layer properties are listed in Table 2.

Table 2. GaN Quasi-Bulk and Drift Layer Properties.

Threading Dislocation Density	~10^{6} cm^{-2}
Quasi-Bulk Doping Level	~10^{18} cm^{-3}
Drift Layer Doping Level	~3x10 cm^{-3}
GaN Thickness	~800 μm

Two different surface cleans were tested in the process in addition to different Schottky metals. The first clean was a piranha etch, a mixture of sulfuric acid H_2SO_4 and hydrogen peroxide H_2O_2, then acetone followed by isopropyl alcohol (IA). The second clean was a hydrofluoric acid etch, hydrofluoric acid (HF) with deionized water at a 1:10 ratio, then acetone followed by IA. The metallization was done primarily via evaporation with sputtering used for the refractory metals. A metal shadow mask composed of six 150 μm-diameter circle contacts in adjacent reticles was used for patterning. Layout of the shadow mask is shown in Figure 13. Designed contact thickness was approximately 200 nm.

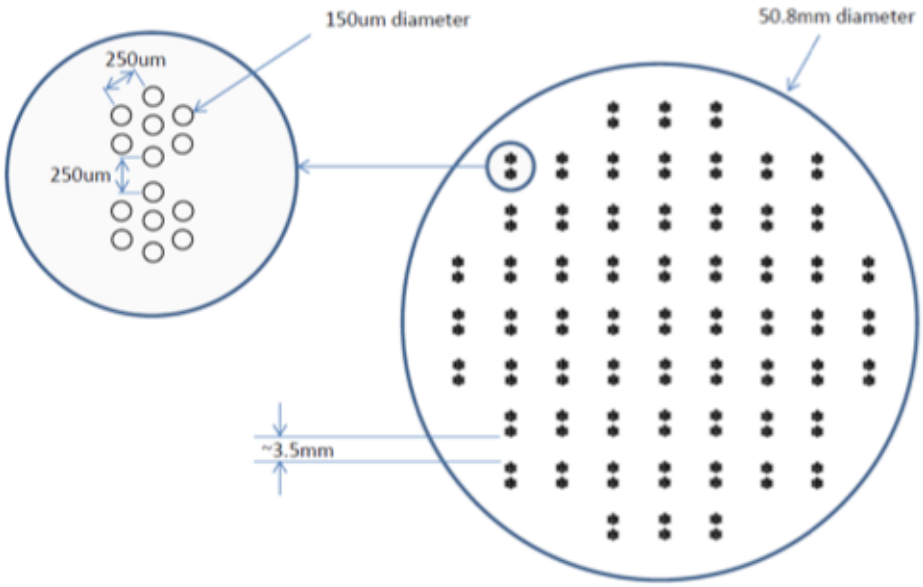

Figure 13. Layout of Metal Shadow Mask used in Metallization of *n*-type GaN Schottky Contacts.

Two factors were considered when choosing the metals. First, for proper Schottky operation on *n*-type GaN, metals with work function greater than 4.8 eV are needed. The 4.8 eV value is derived from the bandgap of GaN, approximately 3.3 eV, plus the electron affinity, approximately 1.5 eV. Second, the solubility of metals into gallium was taken into account based specifically upon whether or not diffusion occurred between the metal and the gallium within the GaN crystal. Based upon these two factors, the following metals were chosen: platinum (Pt), palladium (Pd), molybdenum (Mo),

combination Mo and gold (Au), combination chromium (Cr) and Au, and rhenium (Re). The ohmic back contact was a stack of titanium (Ti), aluminum (Al), tellurium (Tl), and Au and was based upon literature research of known quality ohmic contacts for the N-face, the bottom, of quasi-bulk GaN substrate. A structure diagram of an individual *n*-type GaN Schottky contact is shown in Figure 14.

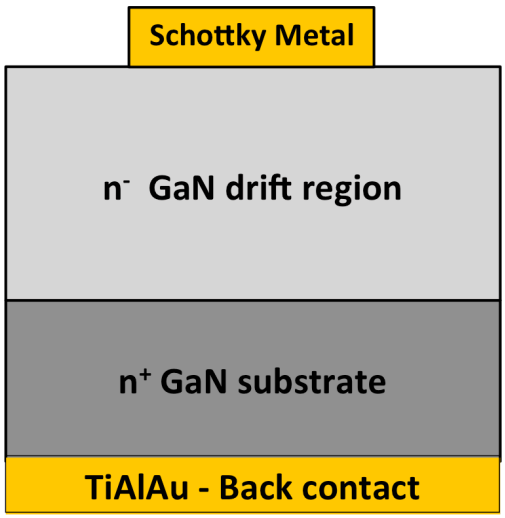

Figure 14. Structure Diagram of Vertical *n*-type GaN Schottky Contact Fabricated at Sandia National Laboratories.

The final partitioned fabricated *n*-type GaN Schottky contacts are shown in Figure 15. P1 is clean 1 Mo and Mo/Au Schottky contacts, P2 is clean 2 Mo and Mo/Au Schottky contacts, P3 is clean 1 Cr/Au Schottky contacts, P4 is clean 1 Pt and Pd Schottky contacts, P5a is clean 2 Pt and Pd Schottky contacts, P6a is Re without O_2 plasma cleaning, P6b is Re with O_2 plasma cleaning, P9 is clean 2 Cr/Au Schottky contacts, and P7 and P8 were not completed.

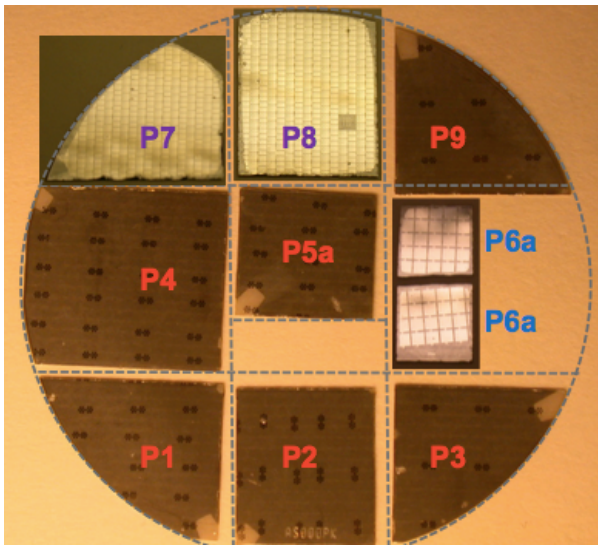

Figure 15. Fabricated Vertical *n*-type GaN-based Schottky Contacts.

B. ELECTRICAL CHARACTERIZATION

1. Current-Voltage Measurements

A six-slot HP4142A Source Monitor Unit (SMU), shown in Figure 16, was used to conduct the I-V measurements of the *n*-type GaN- Schottky contacts. The GaN-based Schottky contacts were placed on a modified Signatone S-1160 Probe Station where tungsten probes were used to establish connection to the anode contacts, as seen in Figure 17. The modified Signatone S1160 thermal chuck served as the cathode contact and was connected to ground. The applied voltage was swept from −5.0 volts to +1.5 volts at an interval of 16.25 mV. A LabVIEW routine was used to interface to the I-V measurement system and to digitally record the data. A block diagram of the I-V measurement system is shown in Figure 18.

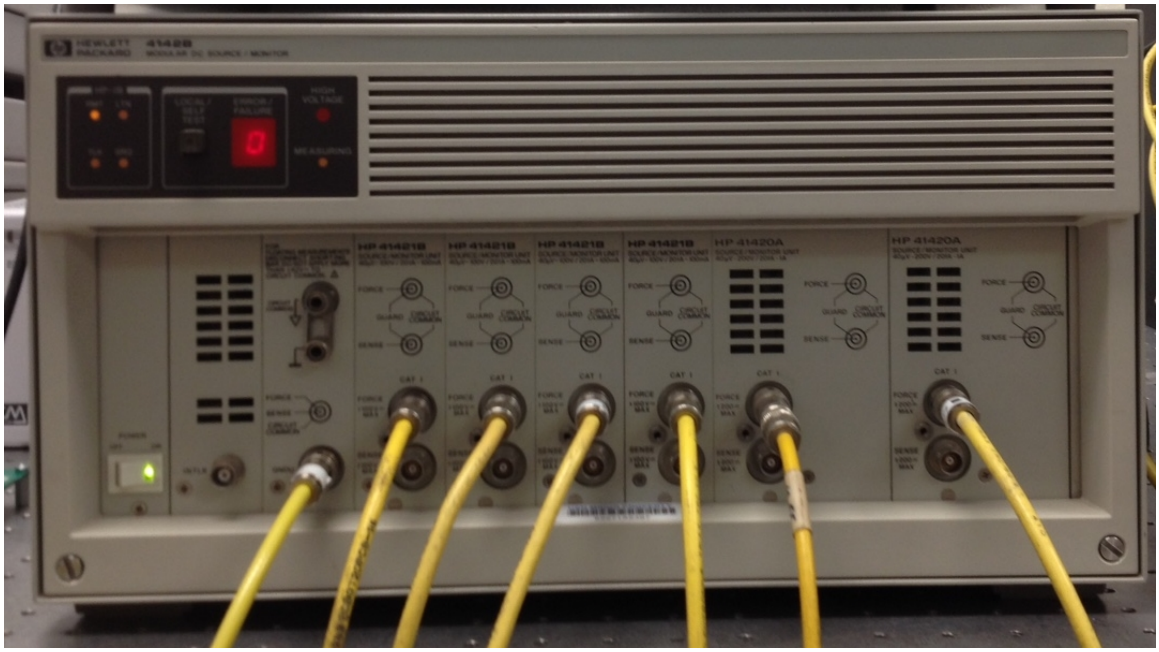

Figure 16. Six-slot HP4142A Source Monitor Unit.

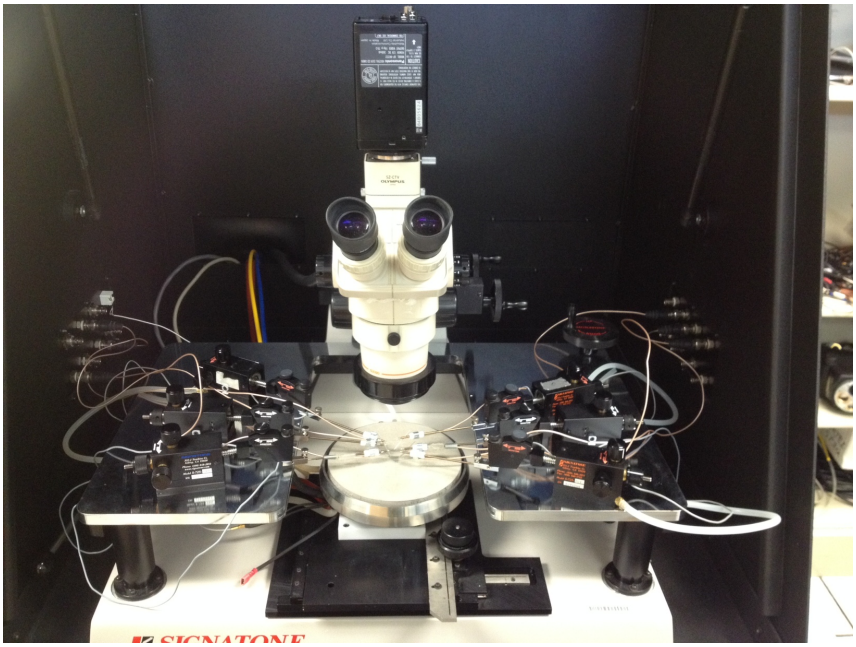

Figure 17. Signatone S-1160 Probe Station used for *n*-type GaN Schottky Electrical Measurements and Accelerated Lifetime Testing.

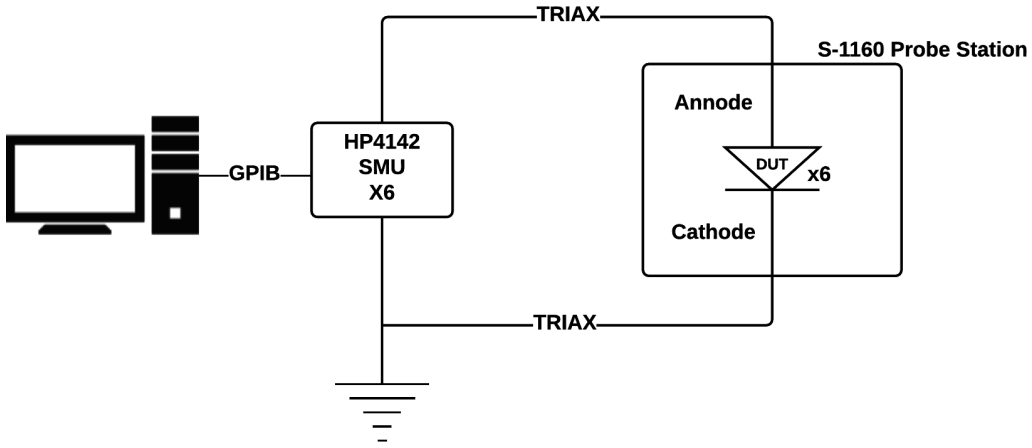

Figure 18. Block Diagram of I-V Measurement System.

2. Current-Voltage-Temperature Measurements

The I-V-T measurements were set up identical to the aforementioned I-V measurement system, as previously seen in Figure 18. In addition, the modified S-1160 Signatone Probe Station's thermal chuck was connected to a Micromanipulator C1000 Heat Exchanger that enabled temperature variation. The temperature was manually controlled via front panel controls on the heat exchanger, as seen in Figure 19. The I-V-T measurement parameters used for characterization are listed in Table 3.

Figure 19. Micromanipulator C1000 Heat Exchanger Front Panel Controls.

Table 3. I-V-T Measurement Parameters.

Temperature Range	30 C to 100 C
Temperature Step	10 C
Applied Voltage Range	−5.0 V to +1.5 V
Voltage Step	16.25 mV

3. Capacitance-Voltage Measurements

A QuadTech 7600 Precision LCR was used to conduct the pre-stress C-V measurements, while an Agilent B1500 Semiconductor Analyzer equipped with a multi-frequency capacitance measure unit (MFCMU) was used to conduct the post-stress C-V measurements. The laboratory arrangement of the QuadTech 7600 Precision LCR and Agilent B1500 are shown in Figure 20. The *n*-type GaN Schottky contacts were placed in a Signatone S-1160 Probe Station where tungsten probes were used to establish connection to the anode contact. The probe station's chuck served as the cathode contact and was connected to ground. The applied voltage was swept from −10.0 V to 0.0 V. A LabVIEW routine was used to interface the pre-stress C-V measurement system and to digitally record the data. The Agilent B1500 software package was used to interface the post-stress C-V measurement system and to digitally record the data. A block diagram of the pre-stress C-V measurement system is shown in Figure 21.

Figure 20. Front Panel Image of Agilent B1500A (top) and QuadTech 7600 LCR (bottom)

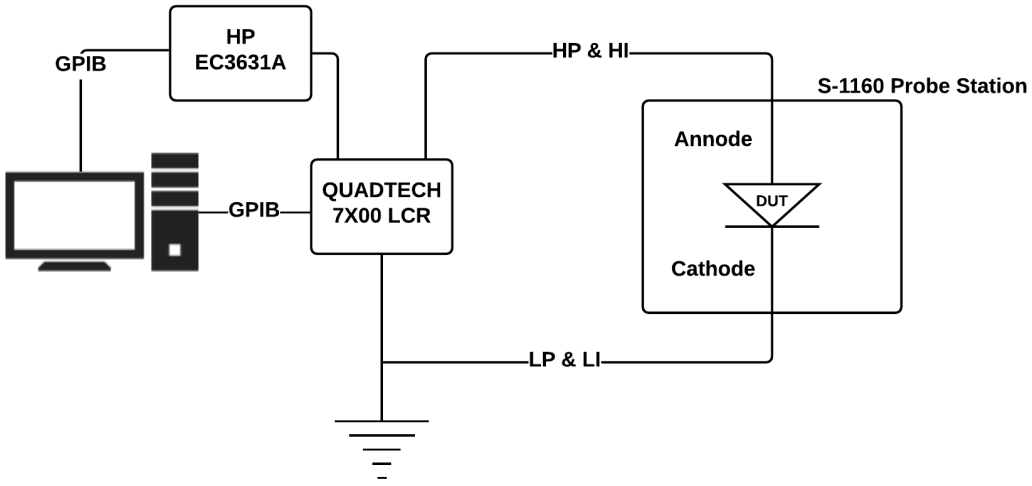

Figure 21. Block Diagram of C-V Measurement System.

C. HIGH CURRENT DENSITY ACCELERATED LIFETIME TEST

The high current density accelerated lifetime test system was constructed from several component systems, as an industry all-in-one stress-measure-stress system does not exist. To accomplish the stress-measure-stress methodology, a switching matrix circuit, shown in Figure 22, was designed to switch between current sources used for electrical stressing and the I-V measurement apparatus. The switching matrix design featured a multiplexing circuit that used Omron G5LE electromechanical relays to multiplex eight probe connections to two SMU signal inputs and eight stress inputs. The switching matrix circuit was a multilayer PCB designed to handle continuous DC current of greater than 5.0 A. The switching matrix circuit schematic is shown in Figure 23. The relay switching was controlled through a TTL compatible input by a National Instrument Data Acquisition module (DAQ), controlled through a USB connection to a computer.

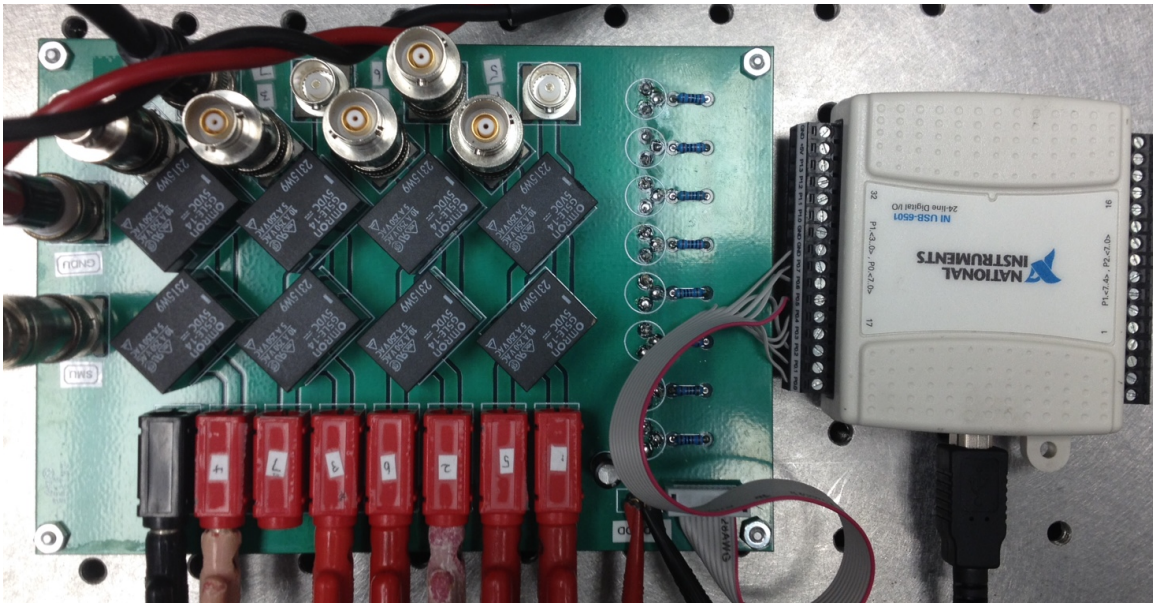

Figure 22. Switching Matrix Circuit (left) and National Instruments Data Acquisition (right) Used in Accelerated Lifetime Test Stress-Measure-Stress System.

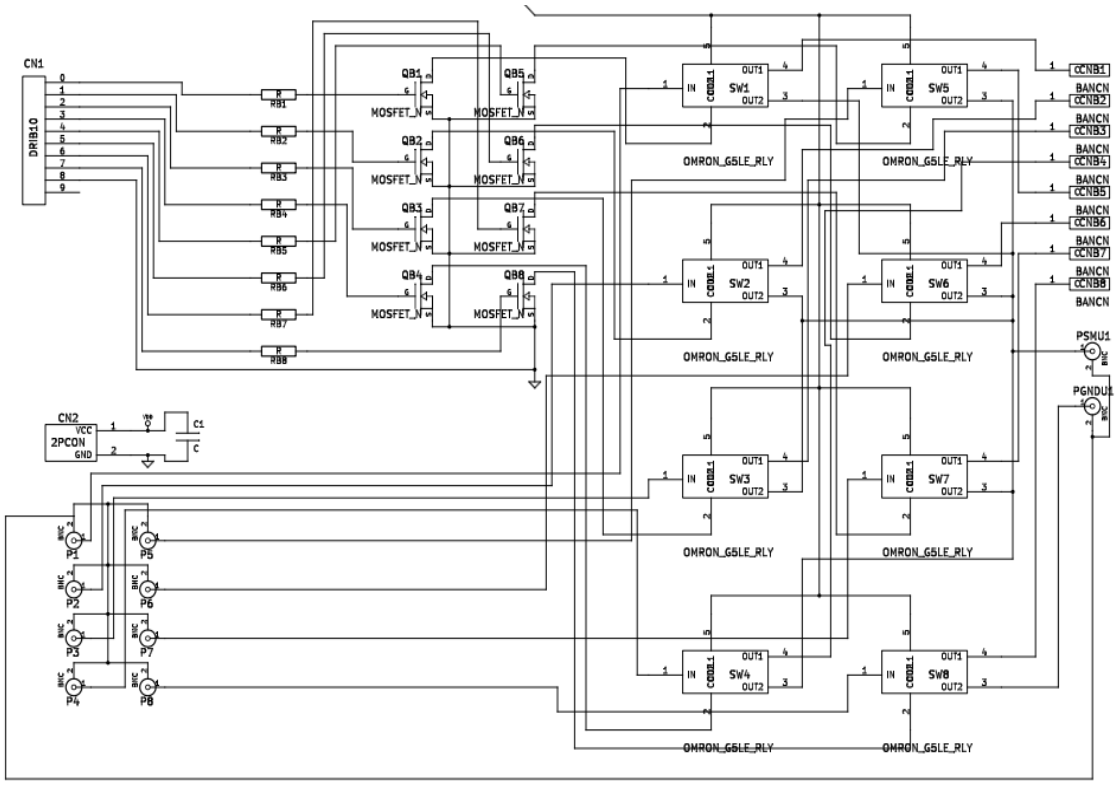

Figure 23. Switching Matrix Circuit Schematic.

Six Agilent EC3631A power supplies, shown in Figure 24, were used to apply constant DC current to the *n*-type GaN Schottky contacts. An additional power supply was used to power the switching matrix. To conduct the measured I-V sweeps, the switching matrix hard switched between the constant DC current source power supplies and a HP4142A SMU, which was used to conduct the I-V measurements. The *n*-type GaN Schottky contacts were placed on a modified Signatone S-1160 Probe Station where six tungsten probes were used to establish connection to the anode contacts of six *n*-type GaN Schottky contacts. The thermal chuck served as the connection to the cathode contact, which was connected to ground. A LabVIEW routine was used to automate and interface the high current density accelerated lifetime test and to digitally record the data. A block diagram of the stress-measure-stress system is shown in Figure 25. The high current density accelerated lifetime test parameters are listed in Table 4.

Figure 24. Stack of Seven EC3631A Power Supplies Used in Accelerated Lifetime Test Stress-Measure-Stress System.

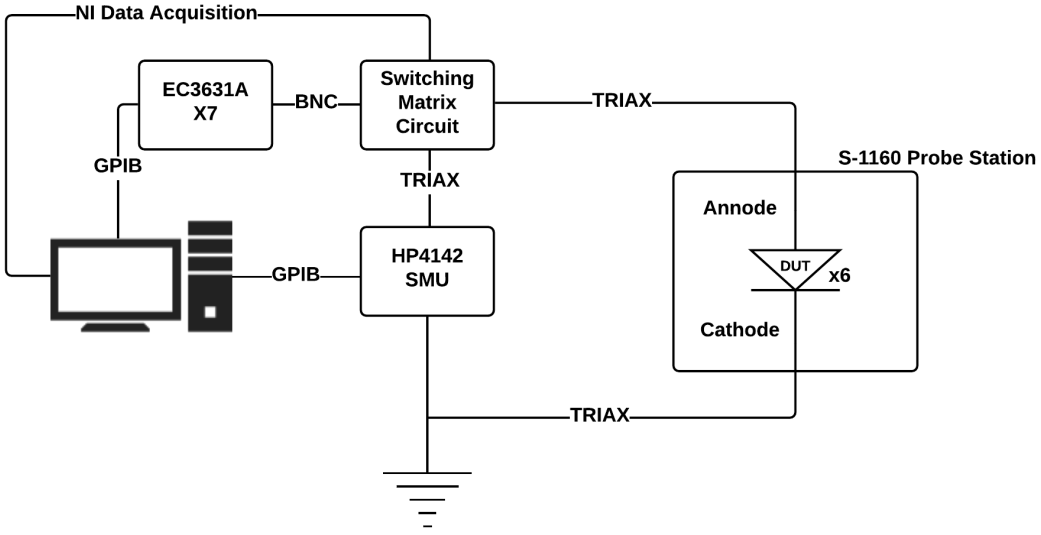

Figure 25. Block Diagram of High Current Density Accelerated Lifetime Test Stress-Measure-Stress System.

Table 4. High Current Density Accelerated Lifetime Test Parameters.

DC Current Density	2.26 kA/cm^2
Stress Duration	168 hrs
Measure Interval	30 min
Temperature	37 C
I-V Applied Voltage Range	−4.0 V to +2.0 V
Voltage Step	10.0 mV

D. POST-STRESS ELECTRON AND OPTICAL MICROSCOPY

1. Scanning Electron Microscopy and Energy Dispersive X-ray Spectroscopy

Morphological features of catastrophic and non-catastrophic degraded GaN-based Schottky contacts were studied using a Zeiss Neon 40 Scanning Electron Microscope (SEM), shown in Figure 26. Coupled with the Zeiss Neon 40 SEM is an INCA 250 Energy Dispersive X-ray Microanalysis system that was used to conduct energy dispersive X-ray spectroscopy (EDS) of the GaN-based Schottky contacts. In this capacity, EDS was used to identify material local changes.

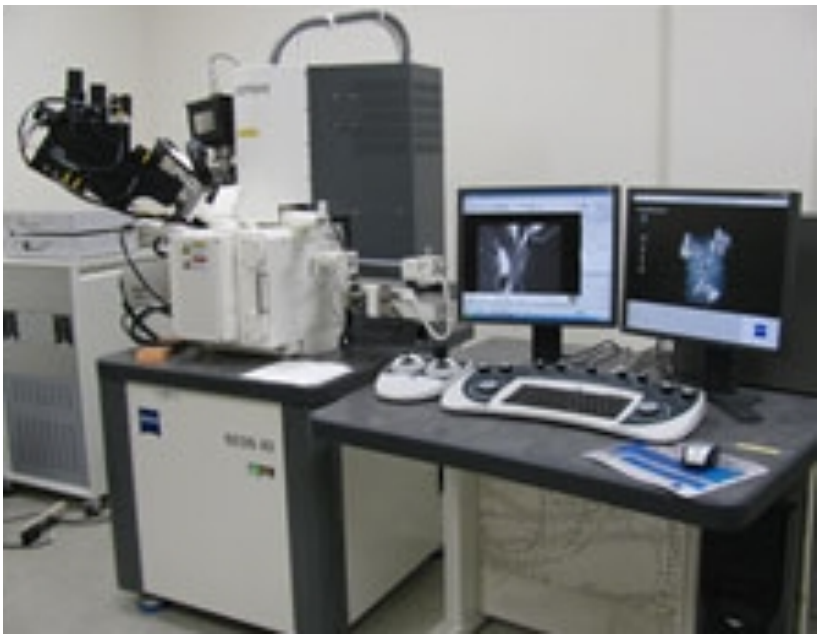

Figure 26. Naval Postgraduate School Scanning Electron Microscope and Energy Dispersive X-ray Microanalysis System.

2. Optical Microscopy

A secondary method of observing morphological changes was executed using a Nikon Epiphot 200 Inverted Metallographic Microscope, as shown in Figure 27. Rudimentary optical imagery analysis was used to identify significant differences between post-stress and pre-stress surface-based morphological conditions.

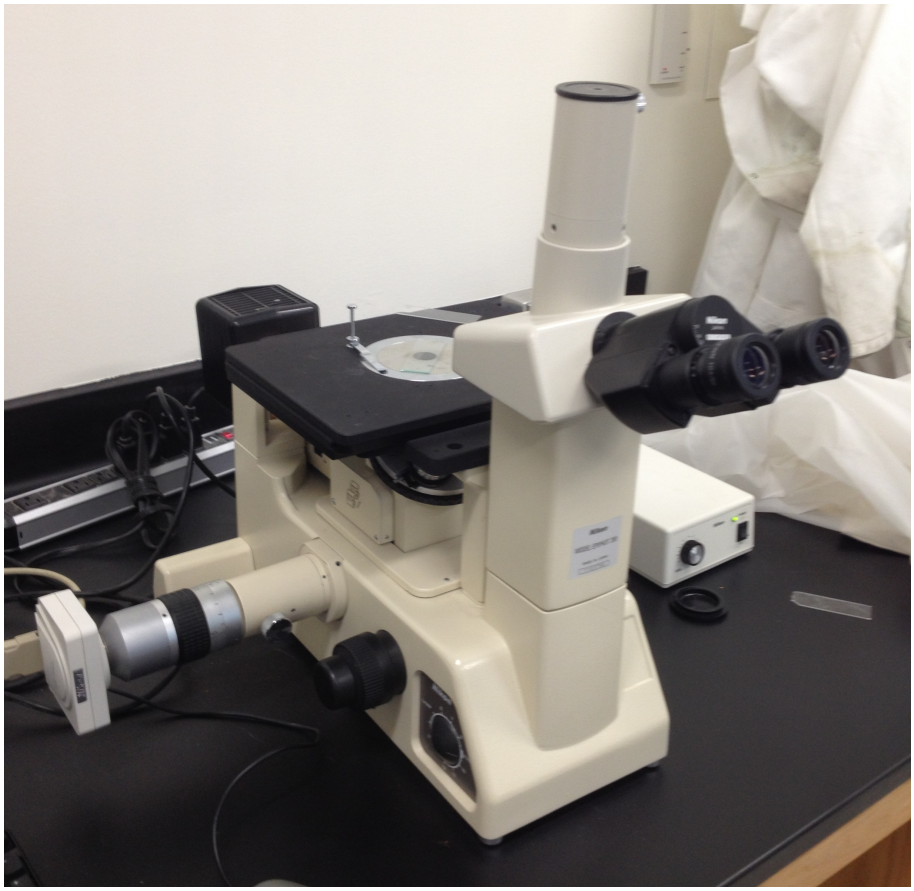

Figure 27. Nikon Epiphot 200 Inverted Metallographic Microscope.

THIS PAGE INTENTIONALLY LEFT BLANK

IV. RESULTS AND DISCUSSION

A. ELECTRICAL CHARACTERIZATION

I-V, I-V-T, and C-V measurements were used to characterize the series of CrAu, Mo, MoAu, Pd, and Pt *n*-type GaN-based Schottky contacts prior to the accelerated lifetime stress test. Measured and derived MS Schottky contact parameters include the doping level N_D, the Schottky barrier height ϕ_b, the ideality factor η, the Richardson coefficient A^{**}, the series resistance R_s, the saturation current J_o, the reverse leakage I_{leak} and the parameters measuring the degree of inhomogeneity. The pre-stress test electrical and material characterization parameters were used as a baseline to identify the quality of the Schottky contacts and for comparative purposes. A complete compilation of the characterization parameters and the measured results are listed in Table 5 and Table 6.

Table 5. GaN-based Schottky Contact Measured Characterization Parameters.

Metal/ Clean	ϕm (eV)	*n*	ϕb (eV)			A**	ND (#/cm3)	Rs (Ω)	Jo (A/cm2)
			I-V	Act. Energy	C-V				
Mo #1	4.6	1.07	0.673	0.523	0.751	15.2	3.1×1016	6.04	1.62×10-4
Mo #2	4.6	1.11	0.615	0.554	0.662	7.55	3.2×1016	58.16	3.64×10-4
Mo/Au #1	4.6	1.03	0.608	0.605	0.664	26.6	4.1×1016	5.29	1.58×10-4
Mo/Au #2	4.6	1.05	0.624	0.539	0.703	1.31	2.5×1016	7.03	1.03×10-4
Cr/Au #1	4.37	1.00	0.586	0.495	0.558	4.92	2.8×1016	2.79	3.46×10-4
Cr/Au #2	4.37	1.12	0.555	0.497	0.655	3.88	2.9×1016	5.97	8.71×10-3
Pd #1	5.15	1.16	1.11	0.867	1.31	0.002	3.4×1016	4.3×10^3	1.05×10-11
Pd #2	5.15	1.10	0.942	0.878	0.98	1.7	1.3×1016	19.1×10^3	5.82×10-10
Pt #1	5.65	1.09	1.06	0.910	1.39	35.7	2.9×1016	1.3×10^3	1.20×10-11
Pt #2	5.65	1.07	1.15	0.978	1.21	5.04	2.2×1016	3.2×10^3	1.61×10-13

Table 6. GaN-based Schottky Contact Lattice Constant and Measured Schottky Barrier Inhomogeneity Parameters.

Metal/Clean	Lattice Structure	a (Å)	σ ($cm^{2/3}$ $eV^{1/3}$)	C_1 (cm^{-2})
Cr/Au #1	BCC	2.88	2.0×10^{-3}	3.0×10^{13}
Cr/Au #2	BCC	2.88	2.2×10^{-3}	6.2×10^{11}
Mo/Au #1	BCC	3.15	2.0×10^{-3}	1.4×10^{11}
Mo/Au #2	BCC	3.15	2.1×10^{-3}	6.5×10^{12}
Mo #1	BCC	3.15	1.9×10^{-3}	1.1×10^{10}
Mo #2	BCC	3.15	2.2×10^{-3}	1.7×10^{9}
Pd #1	FCC	3.89	2.7×10^{-3}	2.3×10^{8}
Pd #2	FCC	3.89	2.1×10^{-3}	1.3×10^{11}
Pt #1	FCC	3.92	1.8×10^{-3}	2.6×10^{9}
Pt #2	FCC	3.92	1.7×10^{-3}	1.8×10^{10}

BCC is Body-Centered Cubic and FCC is Face-Centered Cubic. gallium nitride has a Wurtzite lattice structure with lattice constants a and c of 3.186 Å and 5.186 Å, respectively [32].

1. Schottky Barrier Height

Using the I-V-T measurements, ϕ_b for each Schottky metal and clean type was determined from the corresponding Richardson's plots and Equation (11). The measured ϕ_b for the GaN-based Schottky contacts ranged from 0.49 eV to 0.98 eV. The corresponding measured ϕ_b for CrAu, Mo, MoAu, Pd and Pt clean 1 and clean 2 Schottky metals, respectively, are listed in Table 5. Depicted in Figure 28 are the Schottky barrier height values and associated measurement range bars versus corresponding metal workfunction Φ_m for each Schottky metal.

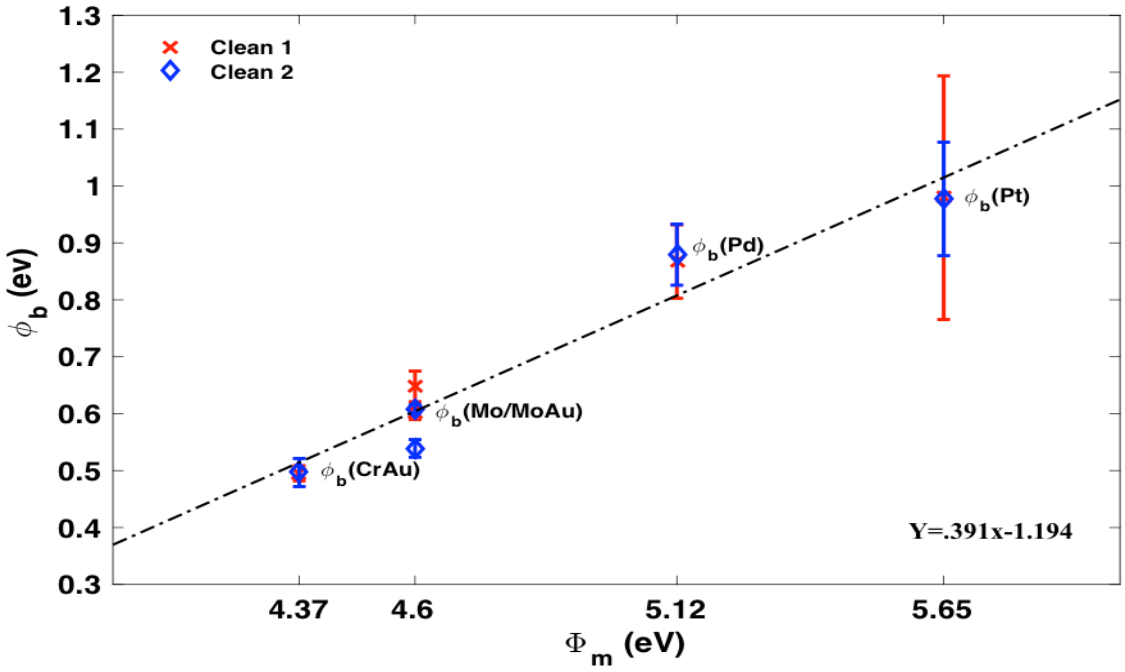

Figure 28. Relation of Measured Schottky Barrier Height to Metal Workfunction.

From the linear fit of the data in Figure 28, it can be seen that the measured Schottky barrier heights deviate from the Schottky-Mott rule as quantitatively expressed in Equation (12). The slope of the linear fit is 0.391, which indicates a certain degree of Fermi-level pinning. This, along with the calculated Schottky barrier height, is consistent with prior research on GaN-based Schottky contacts and is believed to be due to either image force lowering, existence of surface states or SB inhomogeneity due to chemical interactions at the Schottky interface [5, 33]. No observable significant differences existed between the clean types. Unexpectedly though, a wide range of ϕ_b values were observed from the Pt/GaN Schottky contacts.

2. Ideality Factor

From the I-V measurement method, η was determined by plotting J_o versus V_a and using Equation (6) for each Schottky metal and clean type. The measured η for the GaN-based Schottky contacts ranged from 1.05 to 1.20. The corresponding measured η for CrAu, Mo, MoAu, Pd and Pt clean 1 and clean 2 Schottky metals, respectively, are

listed in Table 5. Depicted in Figure 29 are the η values and associated measurement range bars versus corresponding Φ_m.

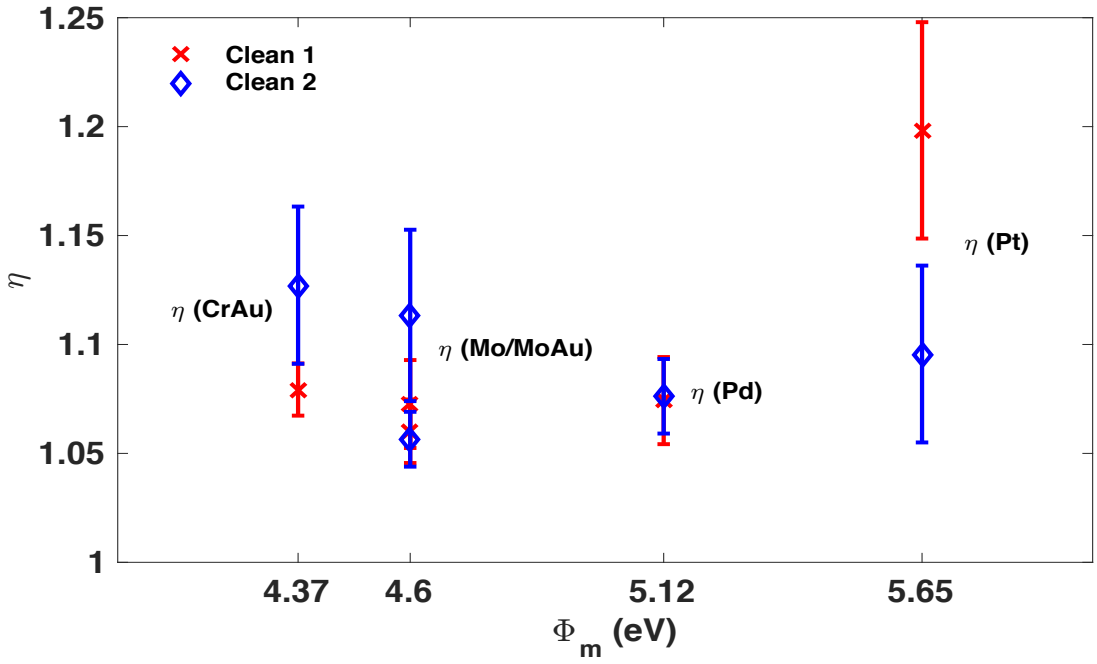

Figure 29. Relation of Measured Ideality Factor to Metal Workfunction.

It can be observed from Figure 29 that clean 1 Schottky metals exhibit η values that are uniform in nature and near a value of one except for Pt, as opposed to clean 2 Schottky metals that, while close to a value of one, exhibit values of η that vary greatly. The value of η is an interface specific parameter and a direct reflection of the adherence of a given Schottky contact to thermionic emission theory. A large degree of variation in η observed in clean 2 is indicative of non-ideal conditions at the metal-semiconductor interface and problems associated with the respective atomic-level bonding.

3. Effective Richardson Constant

An estimation of A^{**} was made from I-V-T measurements. From the *y*-intercept of the Richardson's plot, the mean A^{**} was extracted for each Schottky metal and clean type. The extracted mean A^{**} for the GaN-based Schottky contacts ranged from

0.11 $Acm^{-2}K^{-2}$ to 19.79 $Acm^{-2}K^{-2}$. Listed in Table 5 are the corresponding extracted A^{**} values for CrAu, Mo, MoAu, Pd and Pt clean 1 and clean 2 Schottky metals, respectively. Depicted in Figure 30 are the mean A^{**} values and associated extracted value range bars versus corresponding Φ_m.

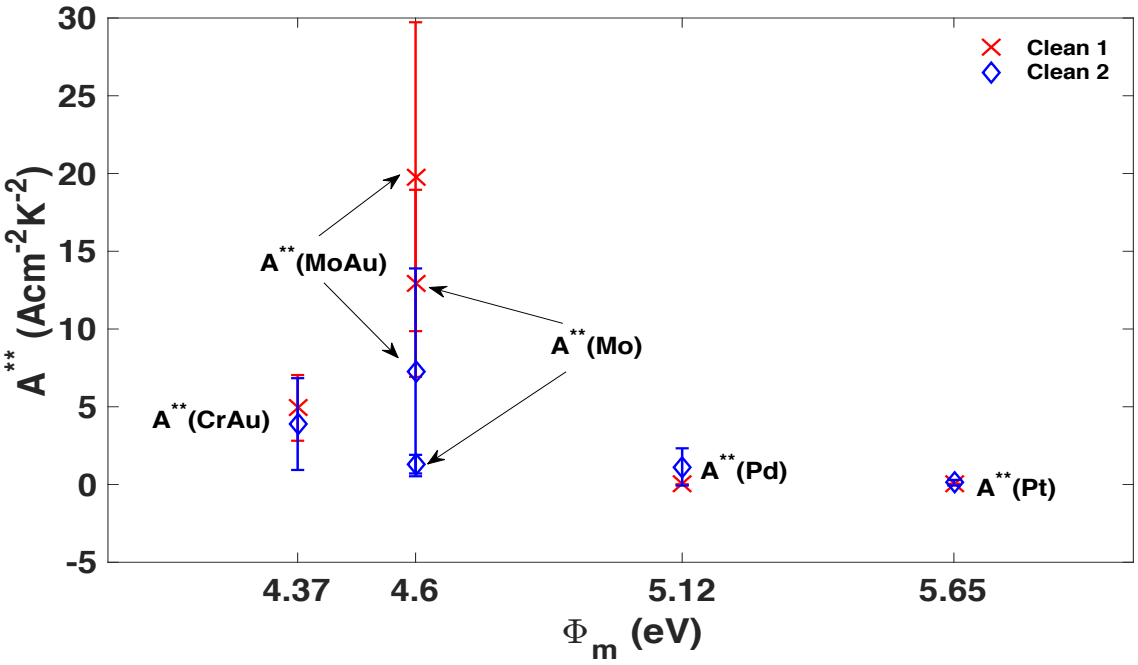

Figure 30. Relation of Derived Richardson's Constant to Metal Workfunction.

It can be observed from Figure 30 that the extracted A^{**} values are significantly smaller than the GaN theoretical value of 26.4 $Acm^{-2}K^{-2}$ for clean 1 MoAu/GaN Schottky contacts, which still exhibit some A^{**} values that are smaller than the theoretical value for GaN; however, previous research has shown that A^{**} for Pt, Pd, and Ni Schottky contacts have similar underestimated values. The low value of measured A^{**} is hypothesized to be indicative of the inhomogeneity and non-ideal nature of GaN-based Schottky contacts [5, 33]. In addition, some research indicates that A^{**} is dependent upon the metal type used in the Schottky junction, further supporting the variation observed in Figure 30 [34].

4. Series Resistance

The R_s values were determined from the I-V measurements for each Schottky metal and clean type by taking the slope within Region III, the series resistance dominated region of the J_o versus V_a plot. The measured mean R_s for the GaN-based Schottky contacts ranged from 2.79 Ω to 19.1 kΩ. Reference Table 5 for the corresponding measured mean R_s for CrAu, Mo, MoAu, Pd and Pt clean 1 and clean 2 Schottky metals, respectively. Depicted in Figure 31 are the mean R_s values and associated measured range bars versus corresponding Φ_m.

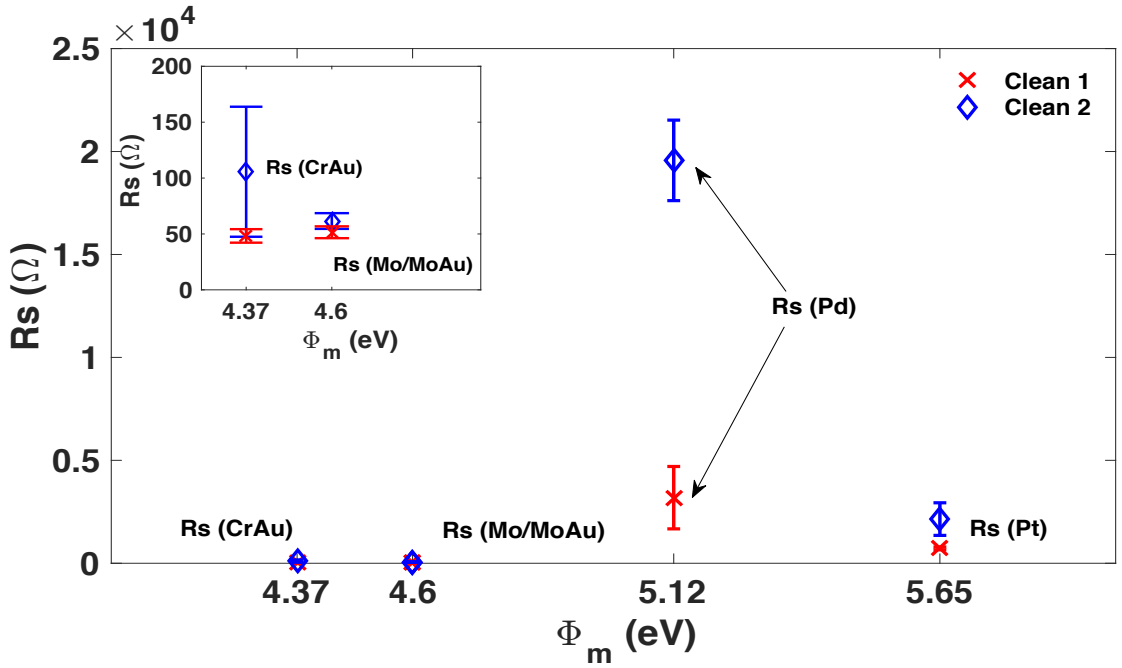

Figure 31. Relation of Measured Series Resistance to Metal Workfunction.

The results of the R_s for CrAu, Mo, and MoAu Schottky metals of clean 1 are observed to be significantly lower than that of the same Schottky metals of clean 2. Both clean types are observed to be within acceptable tolerance levels for Schottky contacts with the same metallization and geometry; however, the series resistances of Pt and Pd Schottky metals of both clean types were found to differ significantly from other metallization. The comparatively high R_s of Pt and Pd Schottky metals indicates a potential lessening of the

effective contact area. Optical imagery of the Pt and Pd Schottky contacts is shown in Figure 32. As observed in Figure 32, the contacts areas seem to have been non-uniform in nature, which is the cause for such a significantly high R_s.

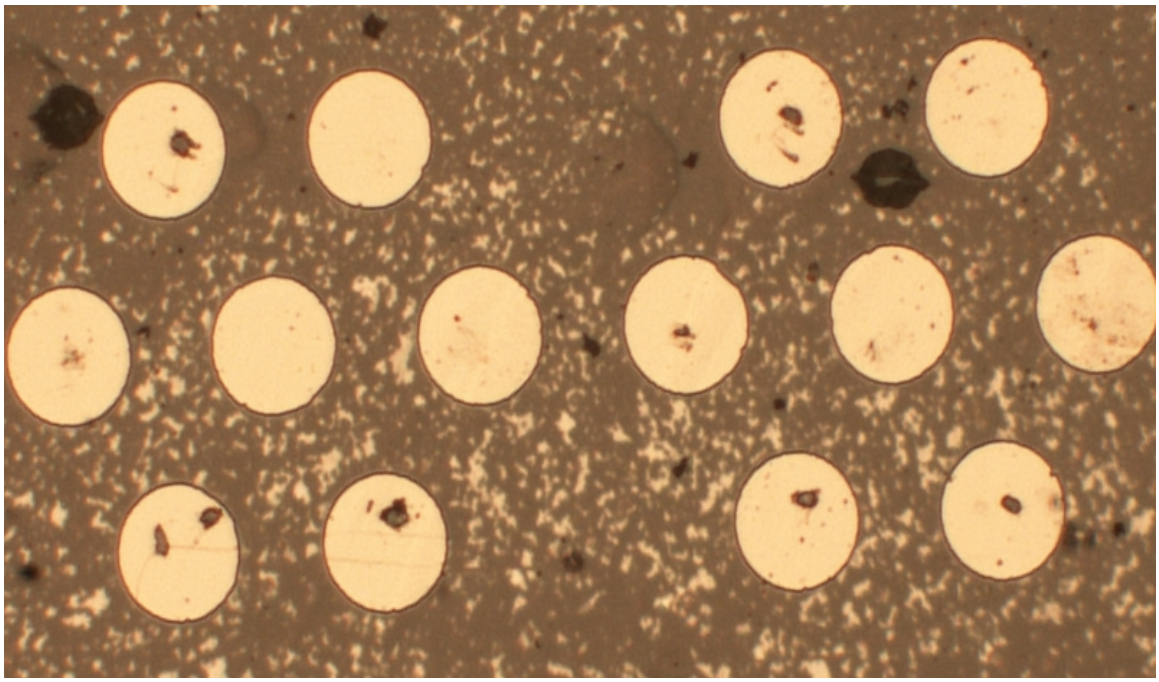

Figure 32. Optical Imagery of Pt and Pd *n*-type GaN Schottky Contacts Showing Non-Uniform Contact Area.

5. Leakage Current

It was possible to determine I_{Leak} from the I-V measurements at room temperature for each Schottky metal and clean type. For uniform comparative purposes, I_{Leak} readings were recorded at an applied voltage of −2.0 V. The resulting measured mean I_{Leak} for the GaN-based Schottky contacts ranged from 2.01×10^{-13} A to 7.03×10^{-7} A. The corresponding measured mean I_{Leak} for CrAu, Mo, MoAu, Pd and Pt clean 1 and clean 2 Schottky metals, respectively, are listed in Table 5. Mean I_{Leak} and associated measured range bars versus corresponding Φ_m are shown in Figure 33.

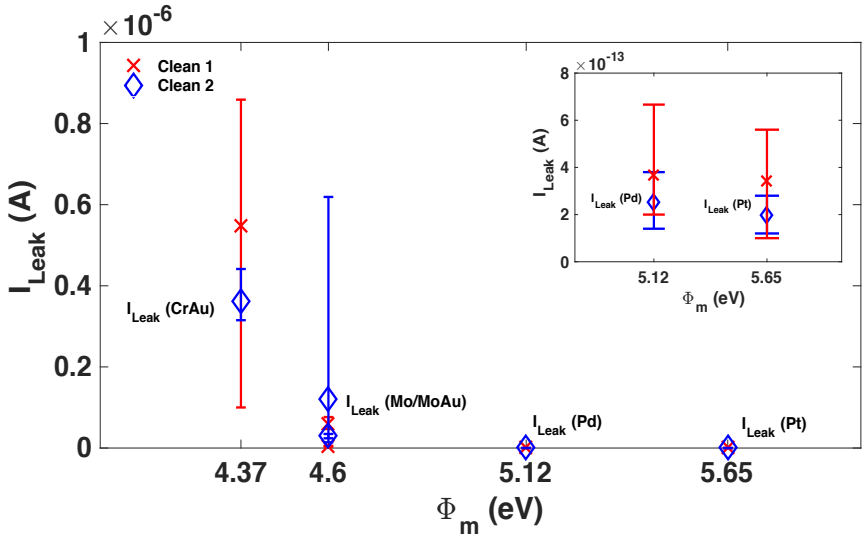

Figure 33. Relation of Measured Reverse Leakage to Metal Workfunction.

The results clearly indicate a significant variation in reverse leakage current across the Schottky metals with CrAu, Mo, and MoAu exhibiting I_{Leak} of several magnitudes greater than for Pt and Pd Schottky metals; however, the values of I_{Leak} all adhere to the expected trend for the chosen Schottky metals on GaN. The leakage current is exponentially proportional to the height of the Schottky barrier. As observed in Figure 33, I_{Leak} follows a general exponential decrease with the increase in metal workfunction, which corresponds to a decrease in the associated Schottky barrier. Of note, I_{Leak} for Pt and Pd Schottky metals may be even lower as the measured values were at the lower limit range of the HP4142 SMU.

6. Schottky Barrier Inhomogeneity Parameters

Using the T_o-based approach to explore Schottky barrier inhomogeneity, we used the I-V-T measurement results to calculate the patch spread parameter σ and patch density parameter C_1 for each Schottky metal and clean type. Depicted in Figure 34 are temperature dependent η values and corresponding T_o approximations for Schottky metals CrAu clean 1(a), CrAu clean 2(b), MoAu clean 1(c), MoAu clean 2(d), Mo clean 1(e), Mo clean 2(f), Pd clean 1(g), Pd clean 2(h), Pt clean 1(i) and Pt clean 2(j).

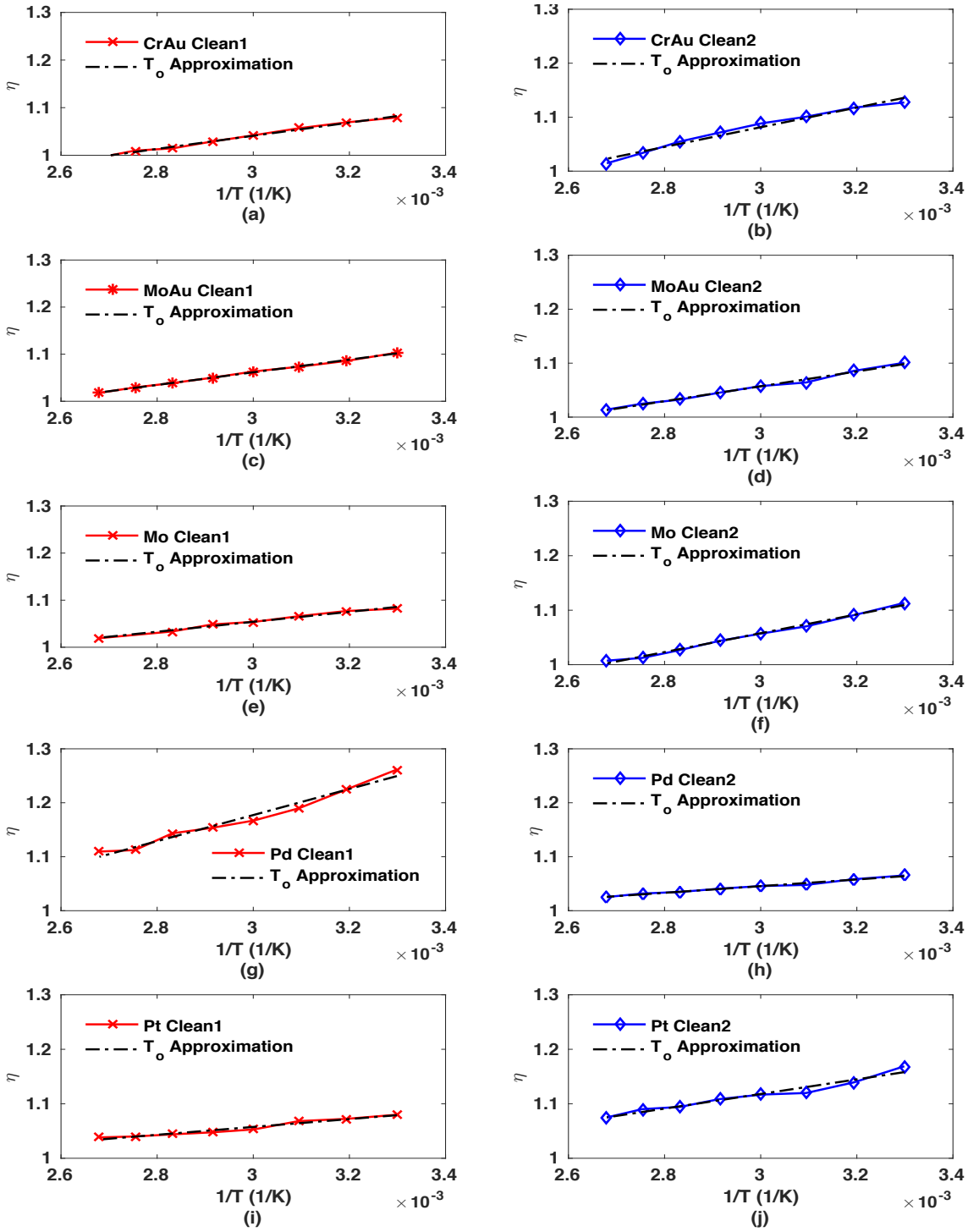

Figure 34. Schottky Barrier Inhomogeneity T_o Anomaly for Temperature Dependent Ideality Factor of Different Metallization and Clean Types.

As observed in Figure 34, the linear rise in η with temperature for each Schottky metal and clean type confirms the existence of Schottky barrier inhomogeneity. Conforming to the Schottky barrier inhomogeneity model, σ was calculated using the linear fit of the T_o approximation for each Schottky metal and clean type. The mean extracted σ values ranged from 0.0017 $cm^{2/3}eV^{1/3}$ to 0.0027 $cm^{2/3}eV^{1/3}$. The corresponding measured mean extracted σ for CrAu, Mo, MoAu, Pd and Pt Schottky metals clean 1 and clean 2, respectively, are listed in Table 6. Shown in Figure 35 are σ values versus corresponding Φ_m.

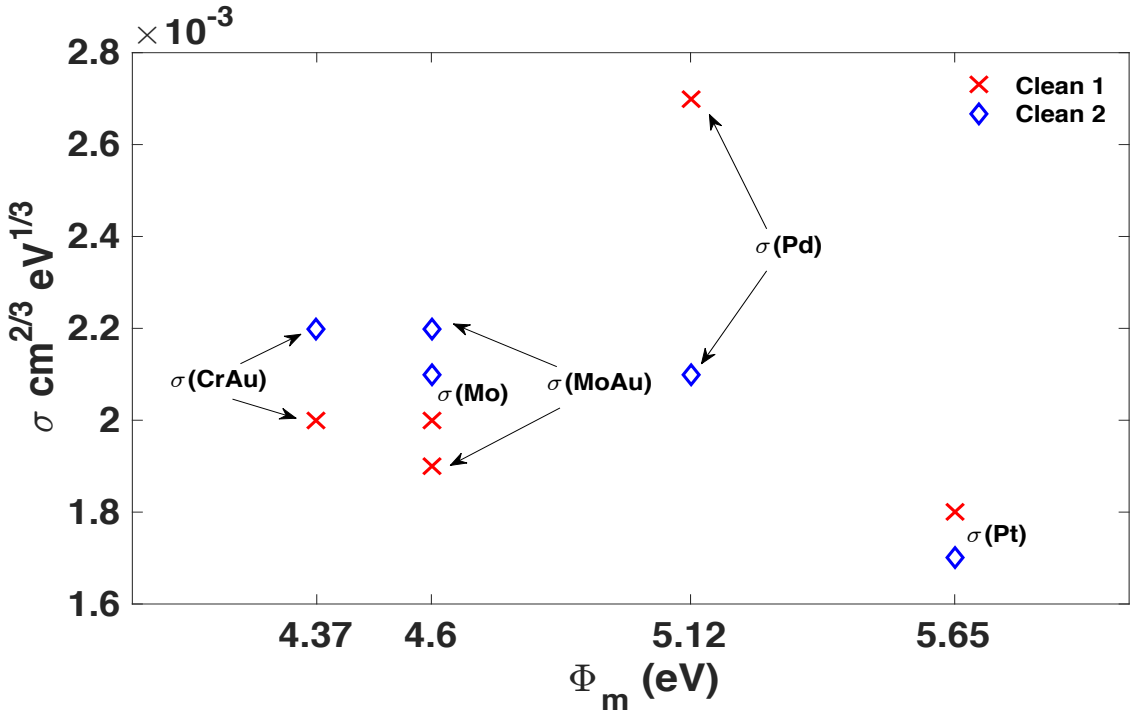

Figure 35. Relation of Schottky Barrier Inhomogeneity Patch Spread to Metal Workfunction.

Based upon the determined σ for each Schottky metal and clean type, C_1 was calculated using Equation (25). The mean C_1 ranged from 1.7×10^{9} cm^{-2} to 3.0×10^{13} cm^{-2}. Reference Table 6 for mean C_1 for CrAu, Mo, MoAu, Pd and Pt Schottky metals clean 1 and clean 2, respectively. Depicted in Figure 36 are C_1 and associated range bars versus corresponding Φ_m.

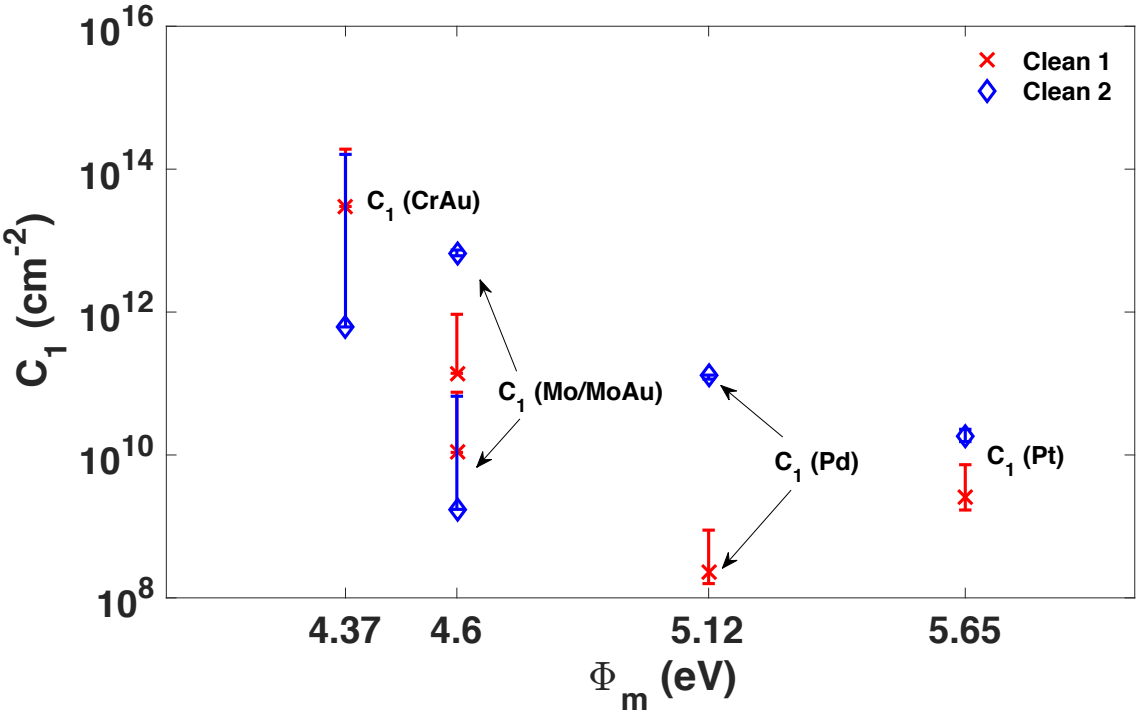

Figure 36. Relation of Patch Density of Schottky Barrier Inhomogeneity to Metal Workfunction.

As observed, the calculated C_1 generally decrease with an increase in metal workfunction. This trend is in line with previous research that also found a direct correlation between C_1 and leakage current [21]. Furthermore, there was a noticeable difference in mean C_1 values between clean types, with clean 1 exhibiting higher mean C_1. The variation in C_1 between clean types combined with the variation in C_1 between each Schottky metal indicates that the choice of Schottky metal and fabrication processes greatly affects the degree of inhomogeneity.

B. IN-SITU DATA

CrAu, Mo, and MoAu Schottky metals clean 1 and 2 were stressed tested according to Table 4 while associated DCIV parameters were tracked throughout the test. Due to the high series resistance associated with Pt and Pd Schottky contacts, those devices were excluded from the accelerated lifetime stress test.

1. Chromium Gold Schottky Metal

Shown in Figure 37 is the applied forward voltage versus time for CrAu clean 1 (a) and clean 2 (b) stressed at 2.3 kA cm^{-2} for 170 hours. The time and respective device numbers that experienced catastrophic failure for clean 1 Schottky metals and clean 2 Schottky metals are annotated in Figure 37(a) and (b), respectively. Generally, it was observed that the forward voltage increased over time for all devices. The significant rise and fluctuation of the forward voltage measured in CrAu clean 1 stress test was due to environmental temperature variations and levels. The temperature fluctuated according to the rise and fall of the room temperature. This problem was fixed for subsequent experiments, which is observed in the smoother measured forward voltages seen throughout the CrAu clean 2 stress test.

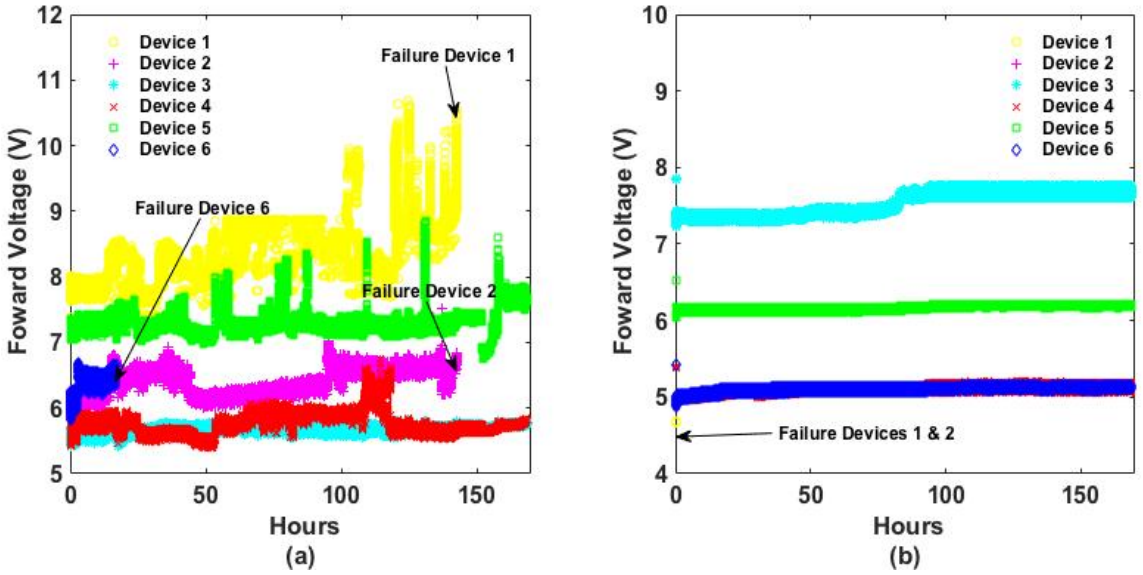

Figure 37. Measured Forward Voltage Throughout 2.3 kA/cm^2 Constant Current Density Accelerated Lifetime Stress Test for CrAu/GaN Schottky Contact (a) Clean 1 and (b) Clean 2.

Depicted in Figures 38, 39, and 40 are ϕ_b, η, and I_{Leak} measurement results versus time for CrAu clean 1 (a) and clean 2 (b), respectively. From the measured device parameters, the CrAu clean 1 ALST results show a slight change in the catastrophically

failed device parameters, while the other surviving devices experienced little change. For the catastrophically failed devices, devices one, two, and six, there was little indication of impending failure as associated device parameters did not show significant degradation prior to failure. It was expected that prior to failure, one would observe a significant decrease in ϕ_b, a significant increase in I_{Leak}, and an increase of η towards a value of two or greater. The only indication of failure was a slight change in the device parameters, of less than five percent compared to baseline, within a few hours of failure. In contrast, the results show significant change in device parameters in the non-catastrophically failed CrAu clean 2 devices. In all cases, except for device six, CrAu clean 2 devices experienced degradation as observed through the decrease in the Schottky barrier height values, significant increase in η, and increase in I_{Leak}. The onset of the degradation was observed to coincide with the immediate catastrophic failure of devices 1 and 2 at the initial commencement of the accelerated lifetime stress test. The degradation ceased at approximately 100 hours with device parameters remaining stable thereafter.

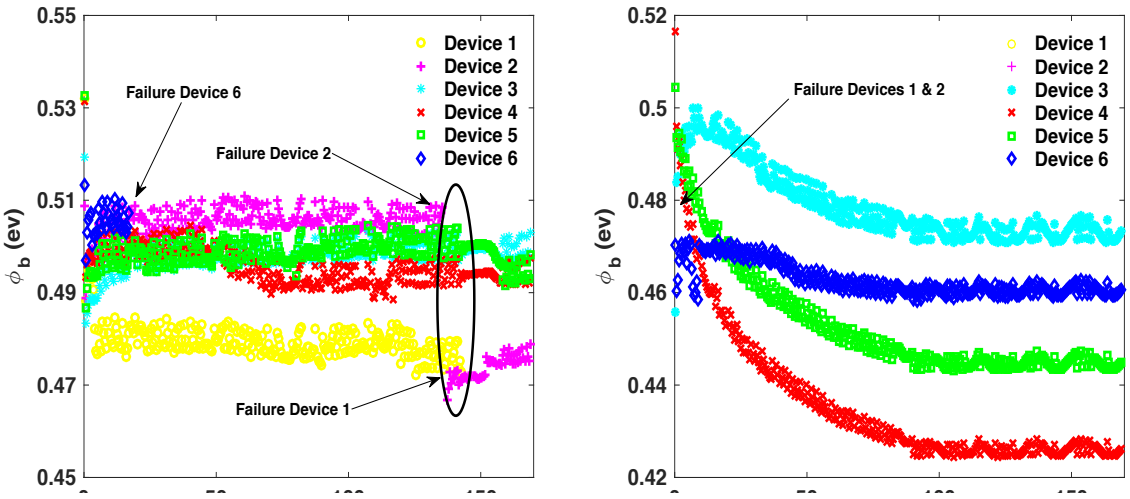

Figure 38. Measured Schottky Barrier Heights throughout 2.3 kA/cm^2 Constant Current Density Accelerated Lifetime Stress Test for CrAu/GaN Schottky Contact (a) Clean 1 and (b) Clean 2.

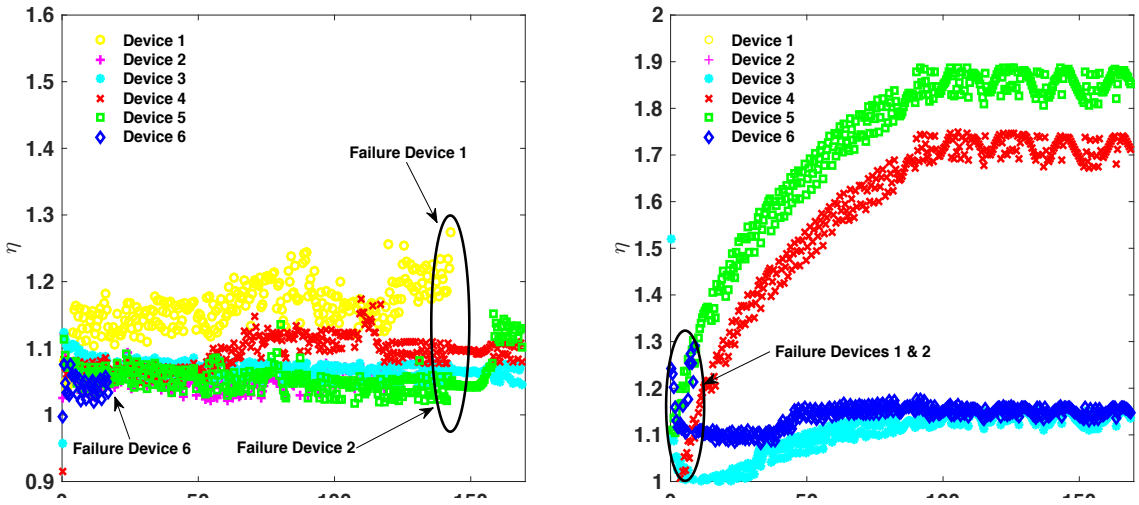

Figure 39. Measured Ideality Factor throughout 2.3 kA/cm^2 Constant Current Density Accelerated Lifetime Stress Test for CrAu/GaN Schottky Contact (a) Clean 1 and (b) Clean 2.

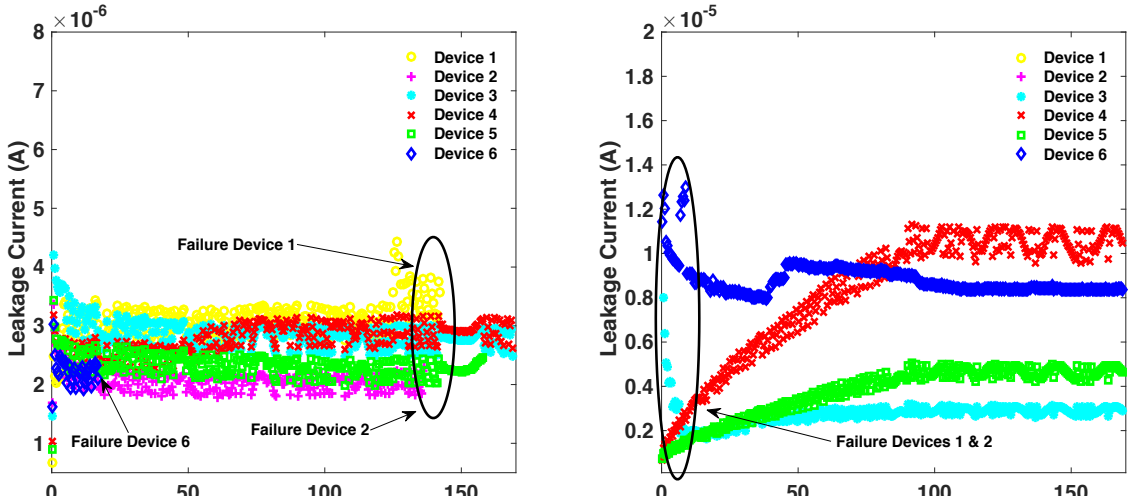

Figure 40. Measured Leakage Current throughout 2.3 kA/cm^2 Constant Current Density Accelerated Lifetime Stress Test for CrAu/GaN Schottky Contact (a) Clean 1 and (b) Clean 2.

Beginning and ending measured device parameter data points for each CrAu/GaN Schottky contact were extracted and a difference was calculated for comparative purposes. For the catastrophic failed devices, ending data points were recorded at the last measurement point prior to failure. Results of this comparison along with device parameter data points are listed in Tables 10 and 11 located in the Appendix.

2. Molybdenum Gold Schottky Metal

Shown in Figure 41 is the applied forward voltage versus time for MoAu clean 1 (a) and clean 2 (b) stressed at 2.3 kAcm^{-2} for 50 hours and 170 hours, respectively. The time and corresponding device numbers that experienced catastrophic failure for clean types 1 and 2 are annotated in Figure 41(a) and (b), respectively. The MoAu clean 1 accelerated lifetime stress test was stopped at 50 hours due to only one device remaining. As observed in Figure 41(a), five MoAu Schottky contacts failed within 30 hours of stress testing. Similar time to failure was observed in the MoAu clean 2 test, as seen in Figure 41(b), where three devices failed within ten hours. Except for the catastrophic failed devices, little significant change was observed in the measured forward voltage in either test. The observed changes in the forward voltage occurred due to fluctuations in series resistance associated with the onset and removal of the catastrophically failed devices from the high current density accelerate lifetime stress test system.

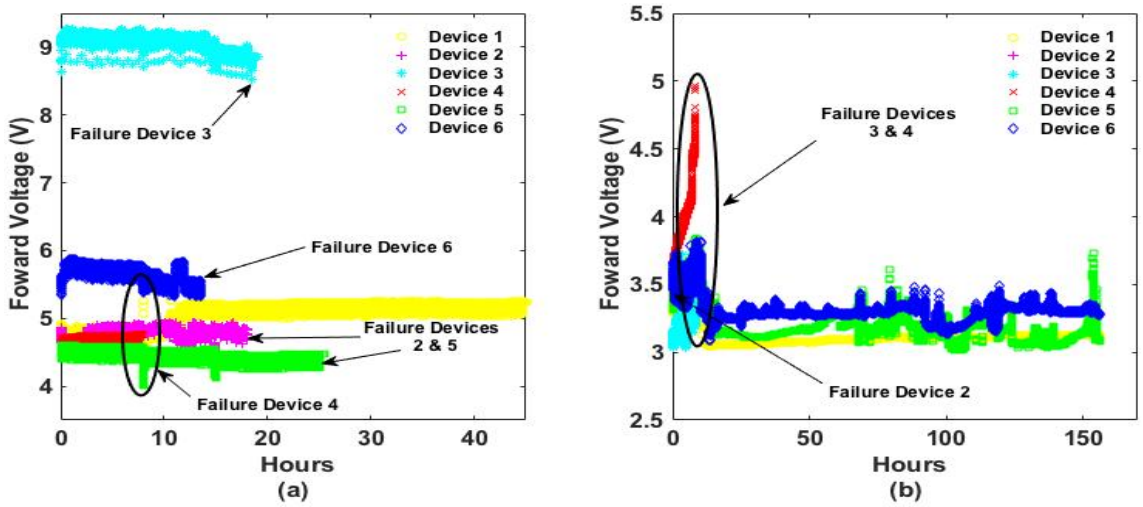

Figure 41. Measured Forward Voltage throughout 2.3 kA/cm^2 Constant Current Density Accelerated Lifetime Stress Test for MoAu/GaN Schottky Contact (a) Clean 1 and (b) Clean 2.

Depicted in Figures 42, 43, and 43 are ϕ_b, η, and I_{Leak} measurement results versus time for MoAu clean 1 (a) and clean 2 (b), respectively. From Figures 42(a) and (b), one can generally observe that both MoAu clean 1 and clean 2 devices experienced a

slight increase in their respective ϕ_b over time. With a general increase in ϕ_b, one expects to observe a corresponding decrease in I_{Leak}, which was the case and is observed in Figures 44(a) and (b). Of note, the immediate and drastic decrease in the Schottky barrier height of MoAu clean 1 device 2, prior to catastrophic failure is likely a result of the device becoming ohmic. Prior experimental work has observed similar transitioning of Schottky contacts to ohmic contacts as a result of stress testing [6]. In Figures 43(a) and (b), changes in η of the catastrophic failed devices are observed, trending to increase slightly all the way up to point-of-failure. For both clean types, the η of the non-catastrophic failed devices changed little except for MoAu clean 2 device one. The η for MoAu clean 2 device one decreased immediately following the simultaneous failure of devices two, three, and four and increased steadily from 1.0 to 1.17 thereafter.

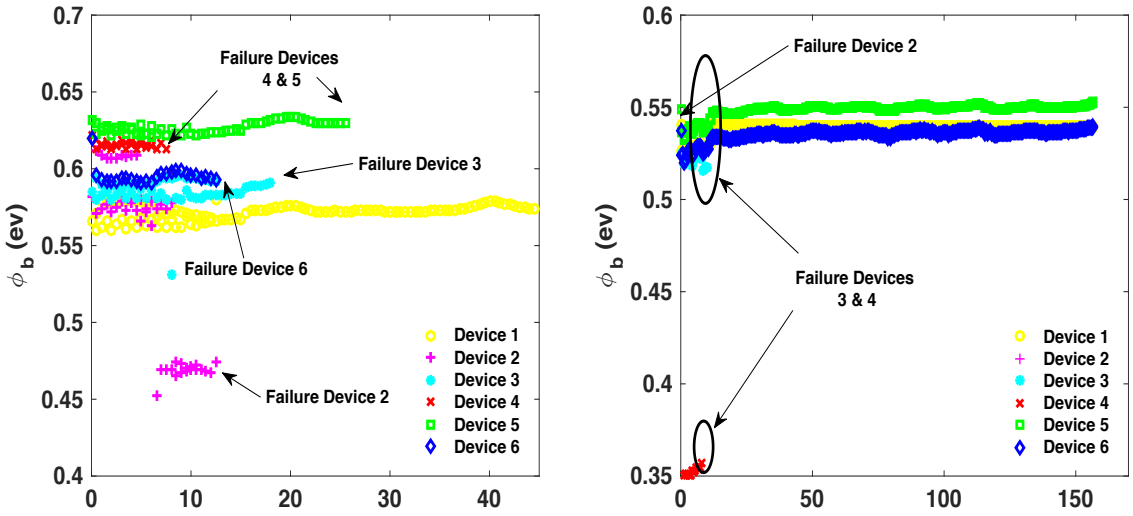

Figure 42. Measured Schottky Barrier Heights throughout 2.3 kA/cm^2 Constant Current Density Accelerated Lifetime Stress Test for MoAu/GaN Schottky Contact (a) Clean 1 and (b) Clean 2.

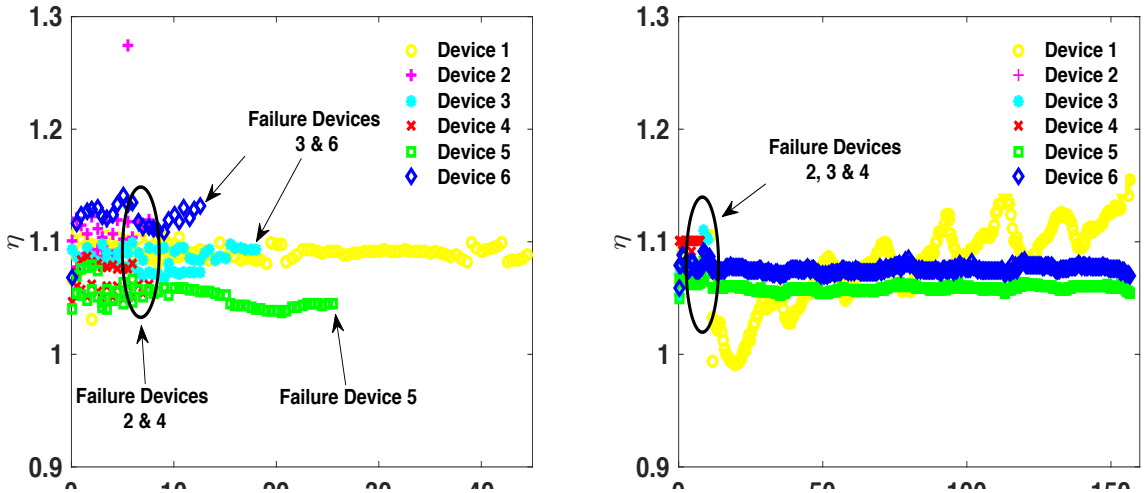

Figure 43. Measured Ideality Factor throughout 2.3 kA/cm^2 Constant Current Density Accelerated Lifetime Stress Test for MoAu/GaN Schottky Contact (a) Clean 1 and (b) Clean 2.

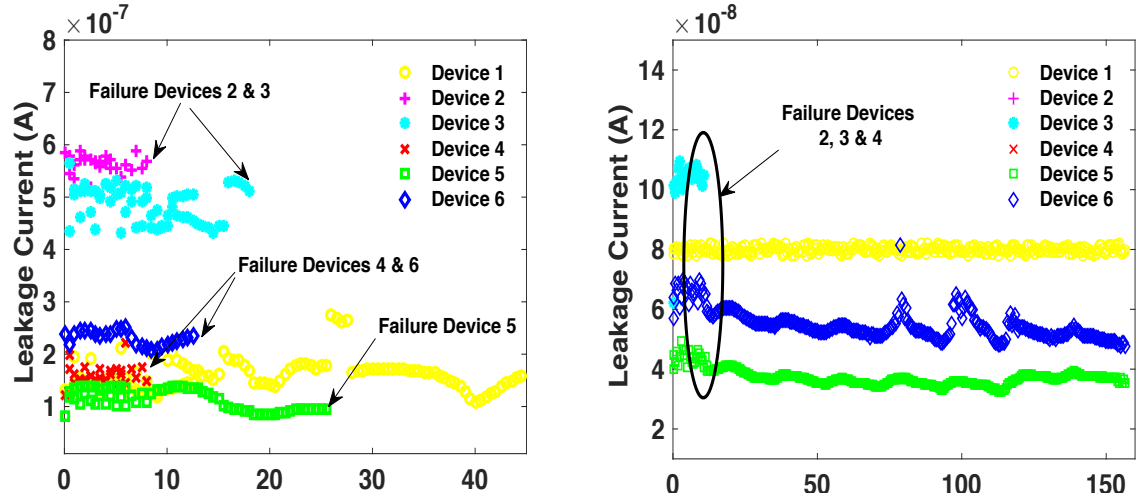

Figure 44. Measured Leakage Current throughout 2.3 kA/cm^2 Constant Current Density Accelerated Lifetime Stress Test for MoAu/GaN Schottky Contact (a) Clean 1 and (b) Clean 2.

Pre- and post-stress device parameter data points for each MoAu/GaN Schottky contact were extracted, and a difference was calculated for comparative purposes. For the catastrophic failed devices, ending data points were recorded at the last measurement point prior to failure. Results of this comparison along with device parameter data points are listed in Tables 12 and 13 in the Appendix.

3. Molybdenum Schottky Metal

Shown in Figure 45 is the applied forward voltage versus time for Mo clean 1 (a) and clean 2 (b) stressed at 2.3 kA cm^{-2} for 170 hours. The time and corresponding device numbers that experienced catastrophic failure for clean types 1 and 2 are annotated in Figure 45(a) and (b), respectively. The forward voltage of the Mo clean 1 devices increased over time, while the forward voltages of the Mo clean 2 devices decreased over time. Annotated on the Figures 45(a) and 45(b) are areas where the measured forward voltages significantly fluctuated. The measured fluctuations coincided with catastrophic failure points. One Mo clean 1 device catastrophically failed, while three Mo clean 2 devices catastrophically failed. All catastrophic failures were observed prior to 100 hours of stress time.

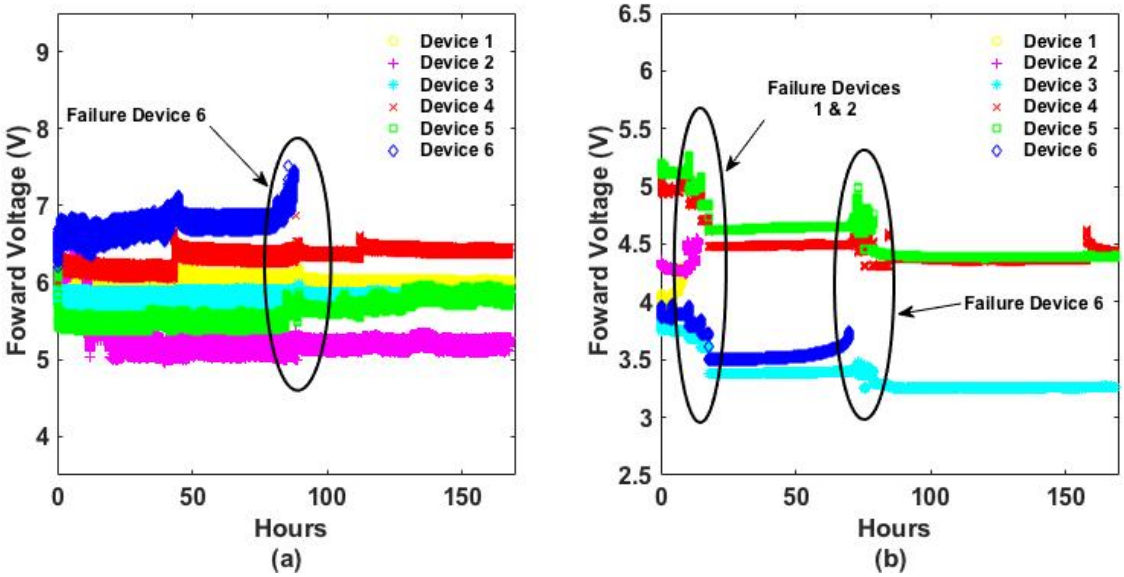

Figure 45. Measured Forward Voltage throughout 2.3 kA/cm^2 Constant Current Density Accelerated Lifetime Stress Test for Mo/GaN Schottky Contact (a) Clean 1 and (b) Clean 2.

Depicted in Figures 46, 47, and 48 are ϕ_b, η, and I_{Leak} measurement results versus time for Mo clean 1 (a) and clean 2 (b), respectively. Observed in Figure 46(a), three Mo clean 1 devices experienced a significant decrease in measured ϕ_b, with device three experiencing a drastic change in measured Schottky barrier height coinciding with

the catastrophic failure of device six. As observed in Figure 46(b), all Mo clean 2 devices experienced an immediate decrease in measured ϕ_b except for device 1. The change in measured ϕ_b of the Mo clean 2 devices was immediate, within the first ten hours, and then the measured ϕ_b stabilized thereafter. These general trends are also observed in the measured η, and I_{Leak} of the Mo clean 1 and clean 2 devices. Depicted in Figures 47 and 47, significant fluctuation and change in several of the device parameters occur at points of catastrophic failure. Mo clean 1 device three experienced a significant change in measured η and I_{Leak} when device six catastrophically failed. Similarly, we observed that a fluctuation in the measured η and I_{Leak} Mo clean 2 devices three, four, and five occurred at the catastrophic failure points of devices one, two, and six. In Figure 48(b), an unexpected general result is observed with the measured I_{Leak} of Mo clean 2. After an immediate increase in measured I_{Leak}, the measured I_{Leak} decreased even though, as seen in Figure 46(b), the corresponding measured Schottky barrier height decreased as well

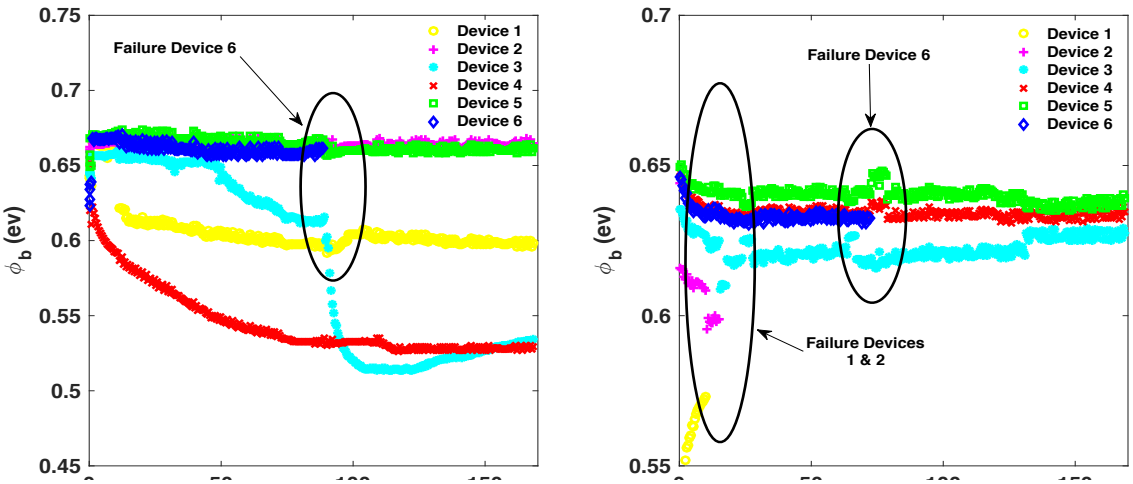

Figure 46. Measured Schottky Barrier Height throughout 2.3 kA/cm^2 Constant Current Density Accelerated Lifetime Stress Test for Mo/GaN Schottky Contact (a) Clean 1 and (b) Clean 2.

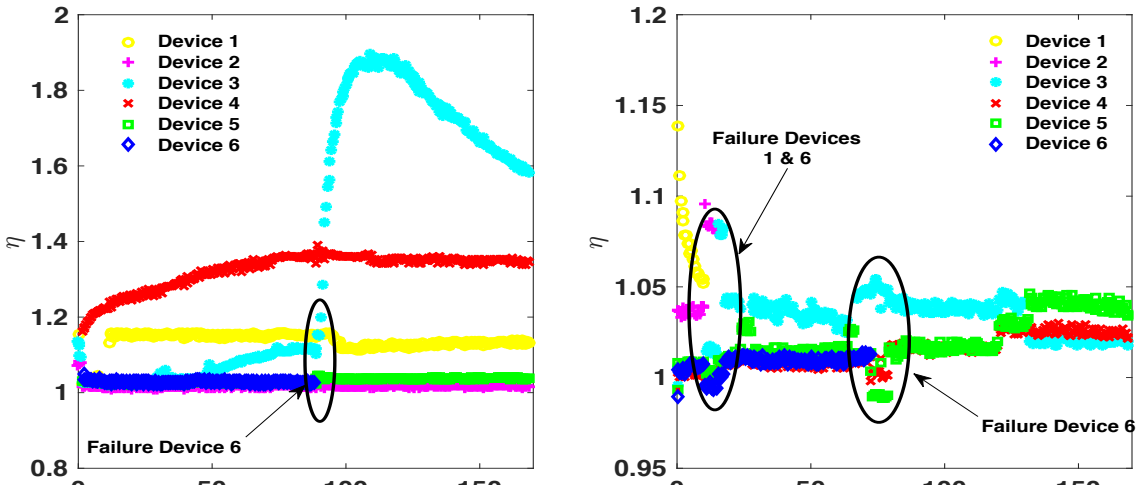

Figure 47. Measured Ideality Factor throughout 2.3 kA/cm^2 Constant Current Density Accelerated Lifetime Stress Test for Mo/GaN Schottky Contact (a) Clean 1 and (b) Clean 2.

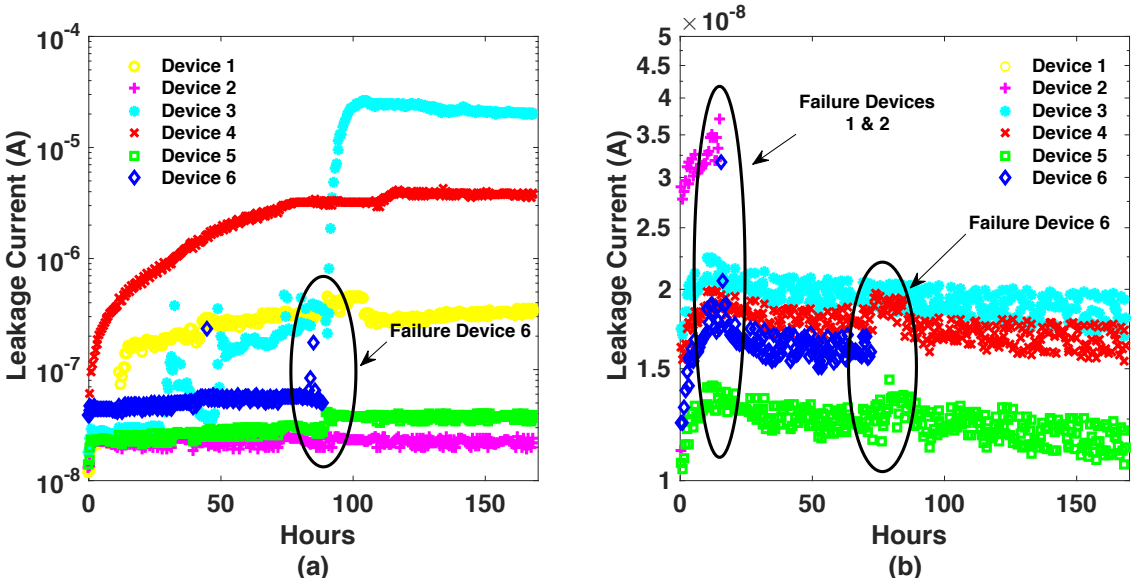

Figure 48. Measured Leakage Current throughout 2.3 kA/cm^2 Constant Current Density Accelerated Lifetime Stress Test for Mo/GaN Schottky Contact (a) Clean 1 and (b) Clean 2.

Beginning and ending measured device parameter data points for each Mo Schottky contact were extracted, and a difference was calculated for comparative purposes. Device parameter data points and percentage of change for Mo clean 1 and clean 2 devices are listed in Tables 14 and 15 in the Appendix, respectively. For the

catastrophic failed devices, ending data points were recorded at the last measurement point prior to failure.

C. POST-ACCELERATED LIFETIME TEST CHARACTERIZATION AND ANALYSIS

I-V-T measurements and rudimentary scanning electron microscopy (SEM) and energy-dispersive X-ray spectroscopy (EDS) were conducted post-stress test. I-V-T measurements were used to determine the existence of a correlation between a change in Schottky barrier inhomogeneity and Schottky contact failure. Electron spectroscopy and EDS were used to identify potential morphological changes and associated degradation mechanisms.

1. Post-Stress Test Current-Voltage-Temperature Measurements—Schottky Barrier Inhomogeneity

Schottky barrier inhomogeneity of the GaN-based Schottky contacts was confirmed through pre-stress test I-V-T measurements and subsequent analysis. The same methodology was used to calculate the degree of Schottky barrier inhomogeneity of each Schottky contact following the high current density accelerated lifetime stress test. From post-stress tested I-V-T measurements of surviving GaN-based Schottky contacts, the inhomogeneity patch spread parameter σ was calculated using the linear fit of the T_o approximation for each post-stress tested Schottky metal and clean type. The mean extracted σ ranged from 0.0020 $cm^{2/3}eV^{1/3}$ to 0.0024 $cm^{2/3}eV^{1/3}$. The corresponding extracted post-stress tested mean σ for CrAu, Mo, and MoAu Schottky metals and clean types 1 and 2, respectively, are listed in Table 7. Shown in Figure 49 are extracted σ measurement results versus corresponding Φ_m.

Table 7. Extracted Post-Stress Tested Schottky Barrier Inhomogeneity Parameters.

Metal/Clean	σ ($cm^{2/3}$ $eV^{1/3}$)	C_1 (cm^{-2})
Cr/Au #1	2.2×10^{-3}	3.3×10^{13}
Cr/Au #2	2.4×10^{-3}	6.5×10^{11}
Mo/Au #1	2.1×10^{-3}	1.8×10^{11}
Mo/Au #2	2.2×10^{-3}	6.7×10^{12}
Mo #1	2.1×10^{-3}	1.4×10^{10}
Mo #2	2.3×10^{-3}	1.9×10^{9}

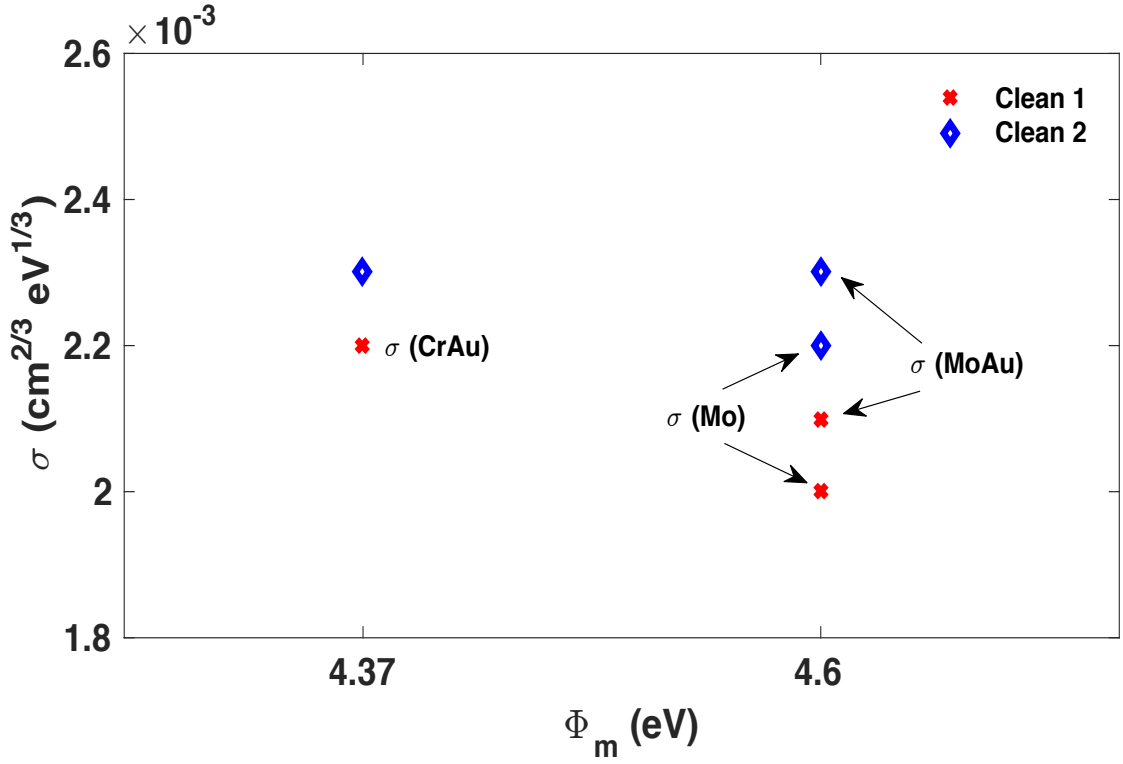

Figure 49. Relation of Post-stress Tested Schottky Barrier Inhomogeneity Patch Spread to Metal Workfunction.

Based upon the determined σ values for each Schottky metal and clean type, C_1 was calculated using Equation (25). The mean C_1 values ranged from 1.9×10^{9} cm^{-2} to 3.3×10^{13} cm^{-2}. Mean C_1 values for CrAu, Mo, and MoAu, clean type 1 and clean type 2,

Schottky metals, respectively, are listed in Table 7. Shown in Figure 50 are C_1 and associated range bars versus corresponding Φ_m.

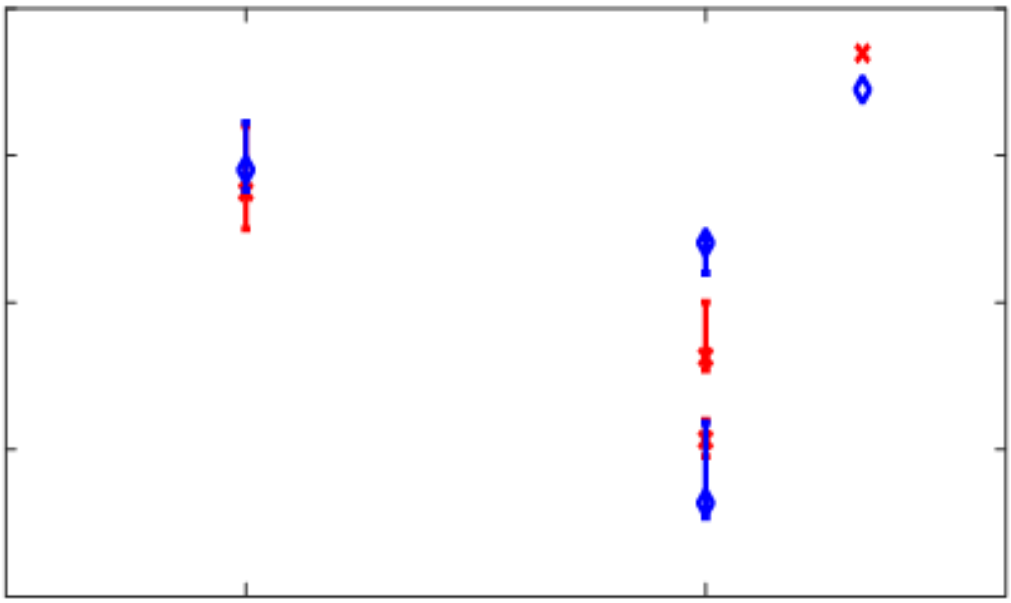

Figure 50. Relation of Post-stress Tested Schottky Barrier Inhomogeneity Patch Density to Metal Workfunction.

Listed in Table 8 is summary of the pre- and post-stress tested σ and C_1, along with percentage change, for each Schottky metal and clean type. The change in the value of σ for the GaN-based Schottky contacts ranged from 4.5 to 10.5 percent, while the change in the value of C_1 ranged from 3.1 to 27.3 percent. As observed in the results, inhomogeneity increased within every Schottky contact regardless of metallization and clean; however, an observed difference existed between clean types. Clean 1 Schottky contacts experienced a greater change in inhomogeneity as compared to clean 2 Schottky contacts. Increases in σ and C_1 are indicative of change occurring at the atomic level of the MS interface between the metal bonds and the gallium bonds. Based upon the results of this research, it is inconclusive as to whether the change is due to the high current density or another experimental factor; however, an increase of barrier height

inhomogeneity, which is the case with an increase in σ and C_1, affects the current transport process and likely reduces long-term reliability of the Schottky contact.

Table 8. Comparative Summary of Extracted Schottky Barrier Inhomogeneity Parameters.

Metal/Clean	Pre-Char. σ ($cm^{2/3}$ $eV^{1/3}$)	Post-Char. σ ($cm^{2/3}$ $eV^{1/3}$)	% Change	Pre-Char. C_1 (cm^{-2})	Post-Char. C_1 (cm^{-2})	% Change
Cr/Au #1	2.0×10^{-3}	2.2×10^{-3}	10.0	3.0×10^{13}	3.3×10^{13}	10.0
Cr/Au #2	2.2×10^{-3}	2.4×10^{-3}	9.1	6.2×10^{11}	6.5×10^{11}	4.8
Mo/Au #1	2.0×10^{-3}	2.1×10^{-3}	5.0	1.4×10^{11}	1.8×10^{11}	12.9
Mo/Au #2	2.1×10^{-3}	2.2×10^{-3}	4.8	6.5×10^{12}	6.7×10^{12}	3.1
Mo #1	1.9×10^{-3}	2.1×10^{-3}	10.5	1.1×10^{10}	1.4×10^{10}	27.3
Mo #2	2.2×10^{-3}	2.3×10^{-3}	4.5	1.7×10^{9}	1.9×10^{9}	11.7

2. Scanning Electron Microscopy and Energy-Dispersive X-ray Spectroscopy

Surface morphology was characterized among catastrophically failed GaN-based Schottky contacts using an optical microscope. Observed from the results of the optical microscopy, there were no noticeable surface morphological differences between optically probed surface morphology clean types or Schottky metals failed devices. Based upon that observation, only one catastrophically failed device from CrAu, MoAu and Mo Schottky metals was imaged and analyzed with the NPS SEM machine. Choosing one from each Schottky metal type allowed for a basic comparison and analysis among Schottky metal types.

Shown in Figure 51 (a) and (b) is an SEM image and corresponding EDS analysis overlay, respectively, of a catastrophically failed CrAu/GaN Schottky contact. Significant damage of the top contact was observed, as visualized in Figure 51 (a). Results from the EDS analysis indicates voiding of the Au, purple, in the degraded region. In addition to a void of Au in the degraded region, Cr was not found as the yellow color indicates the majority presence of gallium (Ga) rather than any metallic overlay. A small presence of oxygen, blue color, is found near the degradation site and is indicative of possible oxidation.

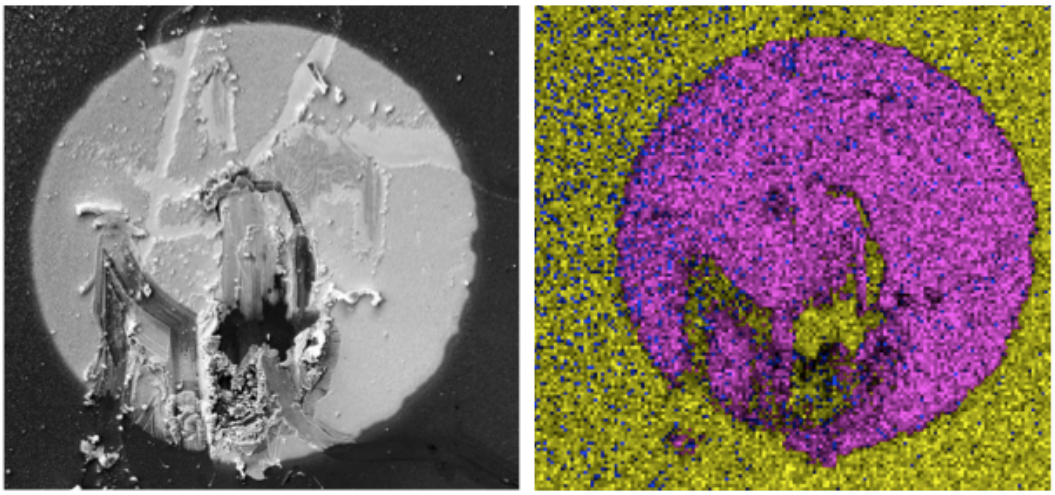

Figure 51. (a) Scanning Electron Microscope Image and (b) Energy Dispersive Spectroscopy Overlay of Catastrophically Failed CrAu/GaN Schottky Contact.

Shown in Figure 52 (a) and (b) is an SEM image and corresponding EDS analysis overlay of a catastrophically failed MoAu/GaN Schottky contact. As was the case with the catastrophically failed CrAu/GaN Schottky contact, significant top contact damage of the MoAu/GaN Schottky contact was observed, as seen in Figure 52 (a). Results from the EDS analysis indicates voiding of Au, aqua blue color, in the degraded region. In addition to a void of Au in the degraded region, only small traces of Cr, purple color, were found. A small presence of oxygen, blue color, and potential oxidation, was found near the degradation site.

Shown in Figure 53 (a) and (b) is an SEM image and corresponding EDS analysis overlay of a catastrophically failed Mo/GaN Schottky contact. As seen with the catastrophically failed CrAu/GaN and MoAu/GaN Schottky contacts, significant top contact damage of the MoAu/GaN Schottky contact was observed, as seen in Figure 53 (a). Results from the EDS analysis indicates voiding of Mo, purple color, in the degraded region. A larger presence of oxygen, blue color, was found around the inner boundary of the degradation site.

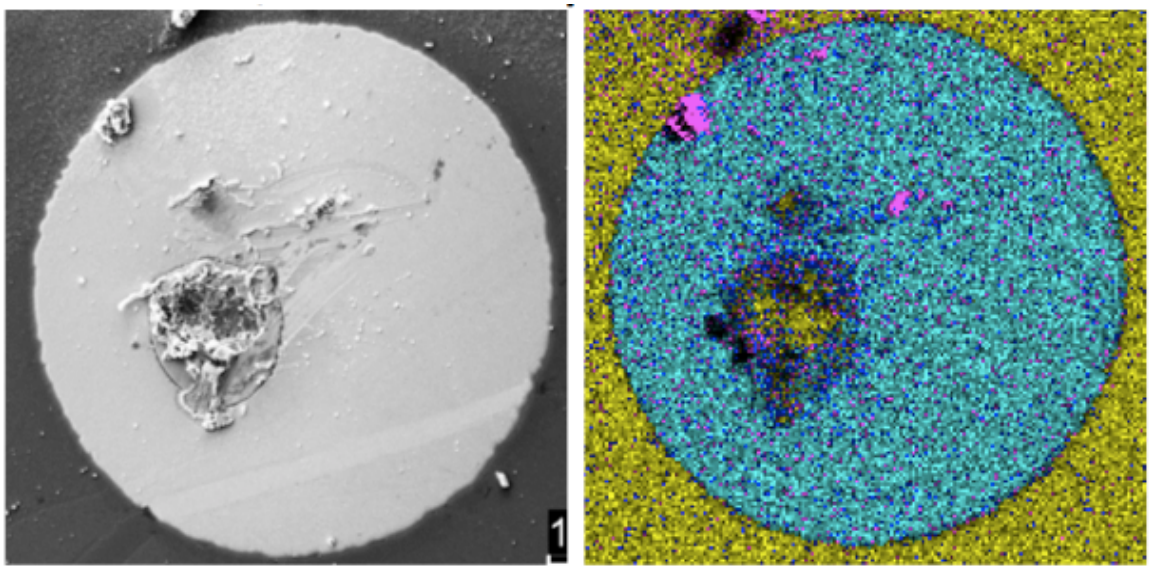

(a) (b)

Figure 52. (a) Scanning Electron Microscope Image and (b) Energy Dispersive Spectroscopy Overlay of Catastrophically Failed MoAu/GaN Schottky Contact.

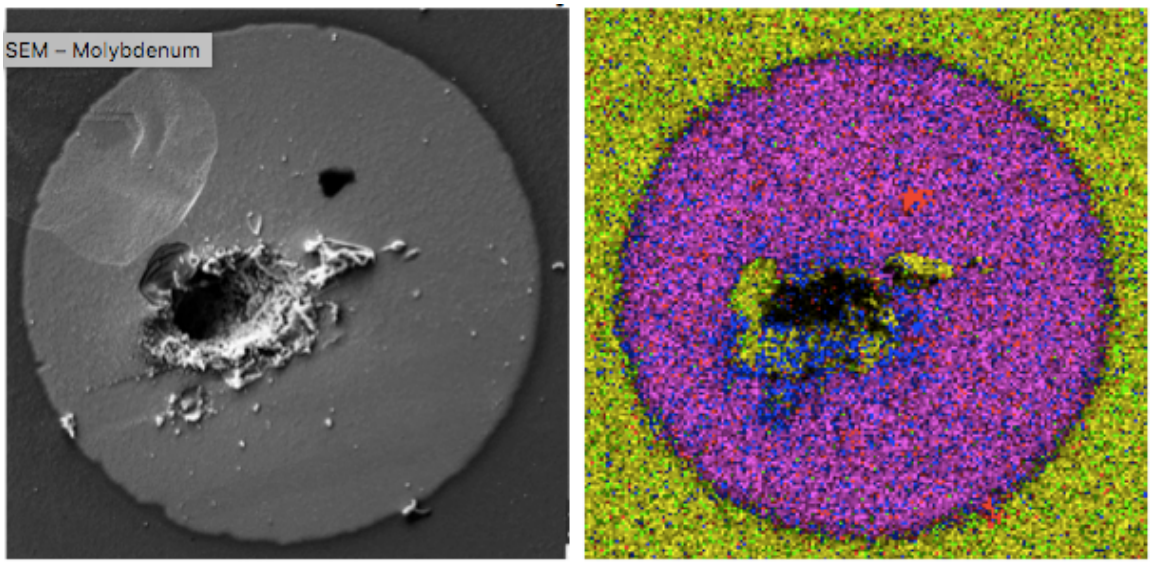

(a) (b)

Figure 53. (a) Scanning Electron Microscope Image and (b) Energy Dispersive Spectroscopy Overlay of Catastrophically Failed Mo/GaN Schottky Contact.

The similarities among the SEM and EDS analysis results of the catastrophically failed GaN-based Schottky contacts confirm that metal diffusion and oxidation occurs during degradation. Metal diffusion and oxidation negatively impact Schottky contact electrical performance through either thermal degradation or charge separation. The degree and rate of which these processes affect the electrical performance of the Sandia fabricated GaN-based Schottky contacts is unknown. Additional research and analysis is required to make a holistic determination of degradation mechanisms.

D. COMPARATIVE ANALYSIS

Six devices of each Schottky metal and clean type were tested. A comparative list summarizing the number of failures, catastrophic and non-catastrophic, and corresponding reliability percentage is presented in Table 9. Average time-to-failure was calculated from the times associated with each catastrophic failure. The average percent change in measured parameter was calculated based upon the non-catastrophic failures.

Table 9. Comparative Summary of Constant DC 2.3 kA/cm^2 Stressed Vertical *n*-type GaN-based Schottky Contacts.

Schottky Metal / Clean	# of Catastrophic Failures	Avg. Time-to-Failure (Hrs)	# of Non-Catastrophic Failures	Avg. % Change in Parameter	# of Reliable Schottky Contacts	Reliability %
CrAu / #1	3	102.3	1	3.1	2	33.33
CrAu / #2	2	0.0	3	48.3	1	16.67
Mo / #1	1	85.0	2	15.2	3	50.00
Mo / #2	3	35.0	0	2.5	3	50.00
MoAu / #1	5	17.5	0	1.5	1	16.67
MoAu / #2	3	5.0	1	7.8	2	33.00

From the comparative results, it is observed that Mo is the most reliable Schottky metal while MoAu is the least reliable. Of the tested clean type 1 Mo/GaN Schottky contacts, one failed catastrophically and two failed non-catastrophically. Between both MoAu clean types, 8 of 10 Schottky contacts catastrophically failed. The majority of failures in MoAu occurred within 20 hours of 2.3-kA/cm^2 stress testing. Secondly, the

results showed that clean 2 enhanced the reliability of Au stacked Schottky metals, while clean 1 was better for bare deposited Schottky metals.

E. IDENTIFIED EXPERIMENTAL CONSTRAINTS

Three experimental constraints were identified during the course of the research that impacts the aforementioned comparative analysis. Electrical arcing was observed during initial testing that caused immediate catastrophic failure. Secondly, joule heating occurred between neighboring Schottky contacts and also at the interface between the contact and probe tip, known as the top contact region. Lastly, Schottky contact topography issues caused bleed over between devices and, as in the case of the Pt and Pd Schottky contacts, prevented the execution of the high current density accelerated life stress tests. Each issue is discussed below.

1. Electrical Arcing

The desired current density stress level for this work was greater than 10 $kAcm^{-2}$; however, that level was not achievable due to arcing between the probe and the metal contact, as depicted in Figure 54. This arcing was observed at current density levels as low as 5.6 $kAcm^{-2}$.

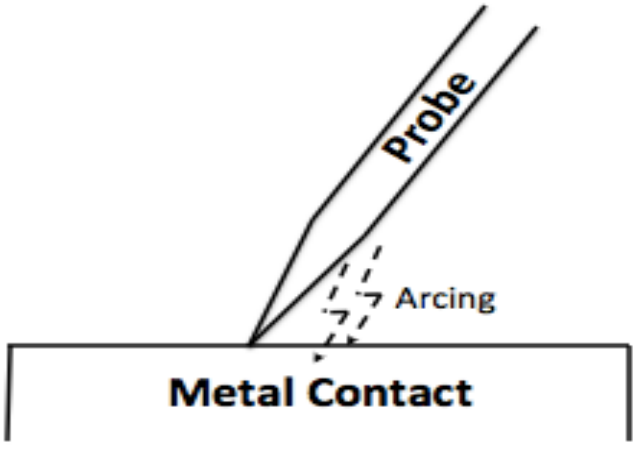

Figure 54. Depiction of Electrical Arcing Between Probe and Metal Contact.

Two leading causes of the electrical arcing are believed to be mechanical instability, wherein the probe lifted off the contact creating a micro-thin air gap between the contact and the probe, and the buildup of charge near the probe tip and subsequent breakdown of the gases in the uncontrolled non-vacuumed test environment. Every occurrence of arcing resulted in the immediate catastrophic failure of the device, as shown and annotated in Figure 55.

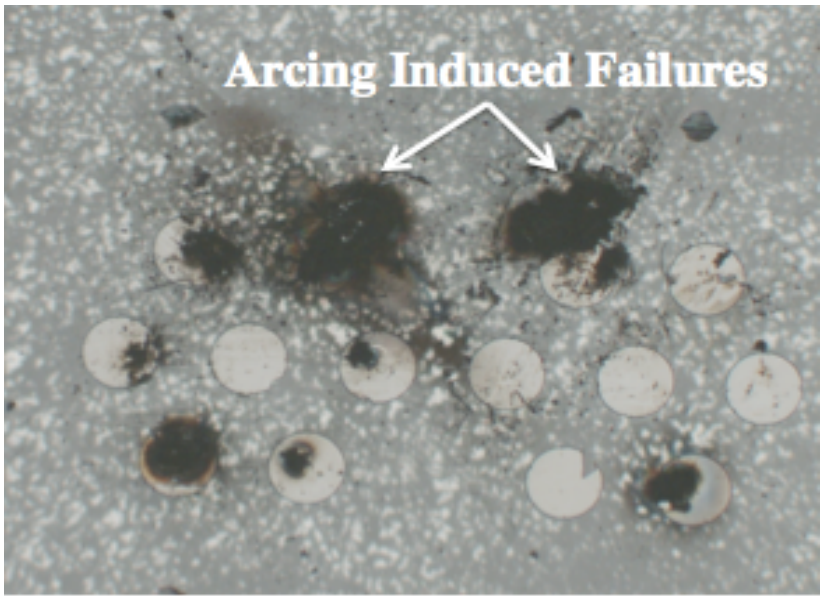

Figure 55. Arcing Induced Failures of *n*-type GaN-based Schottky Contacts.

2. Joule Heating

Joule heating was another source of experimental variation. Using COMSOL Multiphysics software, we made a model of the *n*-type GaN-based Schottky contacts to investigate the cause of the joule heating within the device structure. Because Joule heating is directly related to power dissipation in the Schottky contact, the two areas investigated were the top contact region and the MS junction. The power dissipation associated with the top contact region is a function of the current and the series resistance of the metal, given by

$$P = I^2 R_s . \tag{26}$$

The power dissipation associated with the MS junction is a function of the built-in voltage V_{bi} and the current, given by

$$P = IV_{bi}. \tag{27}$$

Depicted in Figure 56 are the simulated results of the power dissipated in the two regions versus the applied current for the CrAu/GaN Schottky contact. From these results, we observed that joule heating due to the top contact greatly exceeds that of the joule heating associated with the voltage drop across the MS junction. Similar simulation results were produced for Mo and MoAu Schottky metals. Top contact joule heating is problematic when trying to determine and isolate degradation mechanisms associated with high current density stress testing. With the majority of the joule heating occurring at the top contact region, the Schottky contact is being stressed by artificially high operating temperatures rather than being stressed by the applied high current density.

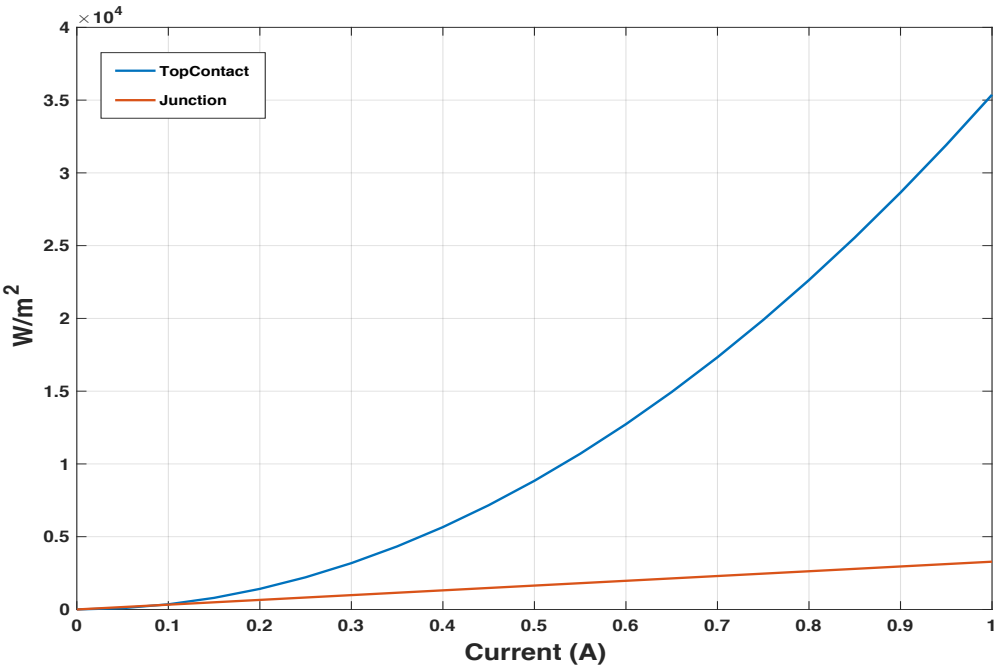

Figure 56. Relation of Power Dissipation Density to Applied Current for *n*-type GaN-based Schottky Contact Areas.

In addition to the joule-heating problem associated with series resistance, neighboring inter-device heating proved to be problematic. Displayed in Figure 57 is a

comparison of Schottky contact device temperature for two different conditions, when only one Schottky contact in a reticle is actively tested and when six Schottky contacts in a reticle are simultaneously tested. The modeling and simulation results show a significant increase in device temperature due to neighboring device stressing. For example, a current of 1.0 A through each device results in a 20 percent increase in temperature when six devices are simultaneously stressed. From the results, we clearly observe that neighbor-induced joule heating is a significant issue that contributes to thermal degradation.

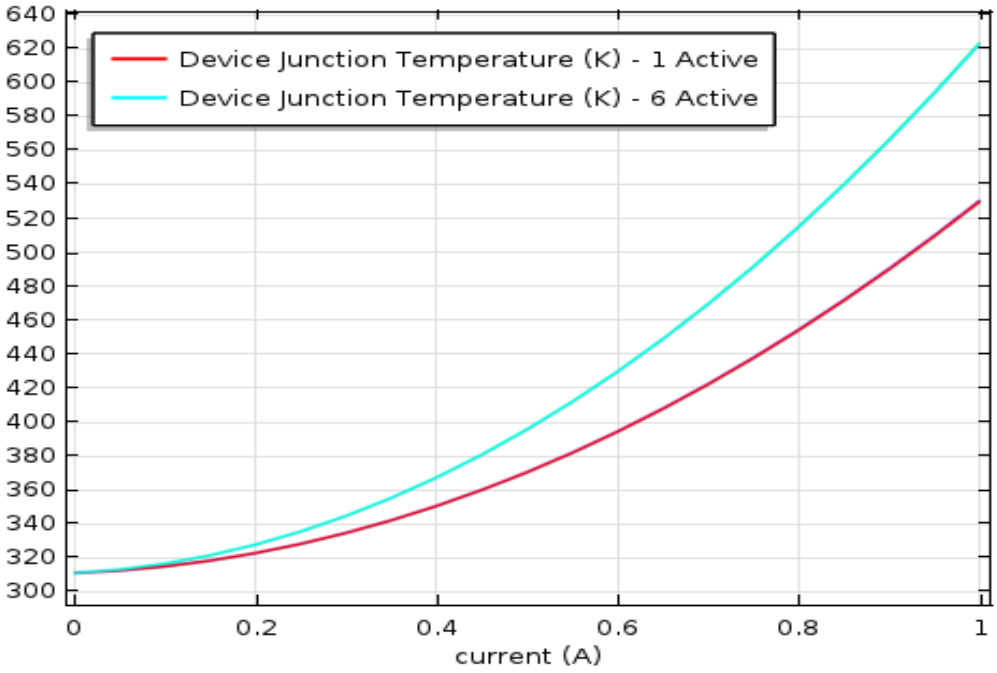

Figure 57. Relation of Junction Temperature to Applied Current for *n*-type GaN-based Schottky Contact Areas.

3. Device Topography

The third set of experimental constraints was associated with the device topography. As aforementioned, the measured high series resistance of the Pt and Pd Schottky contacts precluded those Schottky contacts from being stressed. There exist several possible causes, chiefly among them being the use of a sole shadow mask where

metal contamination or non-uniform deposition may occur. The chosen clean types may also be the cause due to chemical reactions with the Pt and Pd Schottky metals.

Another topography issue, similar to the neighboring joule heating problem, was failure induced bleed over. As observed in the results, when a Schottky contact failed fluctuation in neighboring device parameters occurred. This was most noticeable when a Schottky contact catastrophically failed. Depicted in Figure 58 is visible bleedover that occurred following the catastrophic failure of a clean 1 CrAu/GaN Schottky contact. As observed, visible black colored material was deposited across the entire reticle and onto neighboring Schottky contacts. While this is observed on the surface, it is assumed similar bleed over is occurring within the Schottky contact. We hypothesize that the surface and sub-surface bleed over are a possible contributor to neighboring device parameter fluctuations.

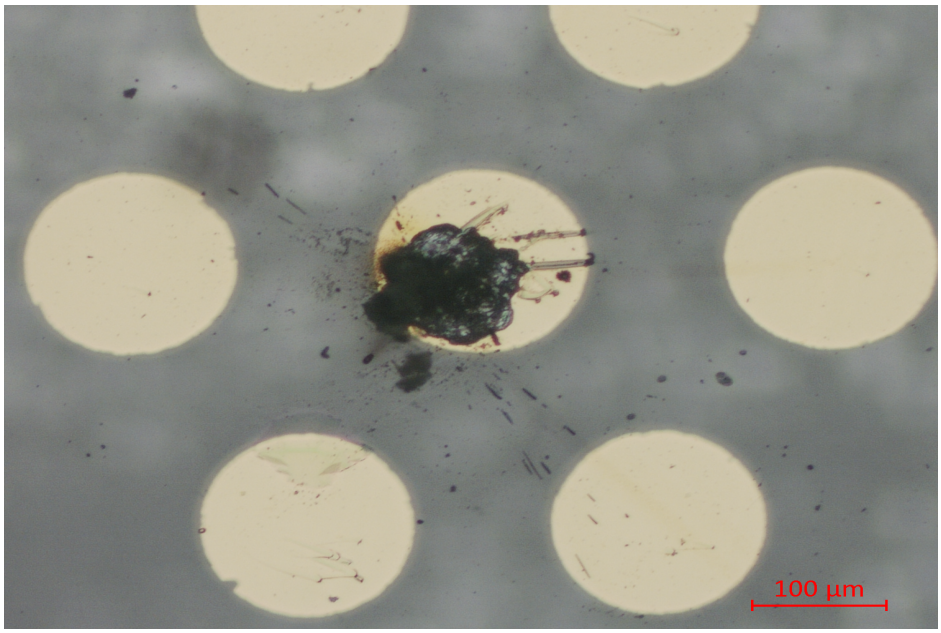

Figure 58. Catastrophically Failed Bleed Over of a Clean 1 CrAu/GaN Schottky Contact.

V. CONCLUSIONS AND FUTURE WORK

A. CONCLUSIONS

The main goal of the research was to compare the reliability of the different Schottky metals and clean types. From the results of the 2.3 kA/cm^2 high current density accelerated lifetime stress test, the vertical clean type 1 Mo/GaN Schottky contact was the most reliable. Clean type 1 and 2 MoAu/GaN Schottky contacts were the least reliable with eight total catastrophic failures. The optical and electron spectroscopy showed significant voiding and contact degradation at the probe tip landing site, the point of highest concentrated current flow.

The aforementioned reliability analysis was great affected by constraints with the experimental setup and non-ideal fabricated vertical *n*-type GaN-based Schottky contacts. The high series resistance, non-ideal fabrication methods, and crowded device patterning limited the allowable current density, caused significant joule heating, and precluded the testing of Pt/GaN and Pd/GaN Schottky contacts. Due to these constraints, additional, and more optimized, testing is required to make conclusive comparisons between Schottky metals and clean types.

In lieu of the constrained stress testing analysis, industry standard electrical measurements of the GaN-based Schottky contacts successfully characterized the devices and provided insight into the degree of inhomogeneity for each Schottky metal and clean type. Overall, measured Schottky barrier heights and associated device parameters of CrAu/GaN, MoAu/GaN, Mo/GaN, Pt/GaN and Pd/GaN Schottky contacts were consistent with prior experimental results [3, 5]. Pre- and post-stress tested T_o anomaly-based inhomogeneity analysis showed a significant increase in the degree of inhomogeneity, with a greater increase occurring in clean 1 Schottky contacts.

B. FUTURE WORK

The next phase of vertical *n*-type GaN-based Schottky contacts need to be optimized for high current density stress testing to achieve a current density of greater than 10 kAcm^{-2}. Specifically, fabrication methods that reduce the series resistance and

ensure uniform Schottky metal deposition need to be used. In addition, the device structure and patterning needs to minimize stressing effects of neighboring Schottky contacts. Packaging the Schottky contacts may also be warranted to assist in isolating individual devices. Addressing these identified experimental constraints will increase the relevant value of collected data and foster more conclusive post-stress test analysis in future testing.

Other spectroscopy techniques can provide additional pre- and post-stress test information and analysis. Photocurrent spectroscopy is a more accurate and direct method of measuring the Schottky barrier height. Admittance spectroscopy and deep-level transient spectroscopy can identify the energy levels of potential traps. The impact of traps on reliability and results of high current density stress testing is unknown and likely device dependent. Detailed transmission electron spectroscopy can provide atomic-level and interface specific region information that can be used to identify degradation mechanisms.

Future testing needs to increase the throughput. Testing only six devices per Schottky metal and clean type, even if results are uncompromised, does not provide enough data points to fit to a mean-time-to-failure model. Fitting to such a model is necessary for predictive analysis and for the realization of a power electronic application specific vertical *n*-type GaN-based Schottky contact. In addition, increased data points will better inform the computer aided modeling of the vertical *n*-type GaN-based Schottky contacts. Accurately modeling and simulating the Schottky contacts will validate future experimental findings.

APPENDIX. SCHOTTKY CONTACT DEVICE PARAMETER DATA

Table 10. CrAu/GaN Schottky Contact Clean 1 Measured Device Parameters.

Dev. #	Ideality factor n			SBH ϕ_b (eV)			Leakage Current I_{Leak} (A)		
	Before	After	% diff	Before	After	% diff	Before	After	% diff
1	1.110	1.22	9.91	0.48	0.47	-2.08	3.77×10^{-6}	2.48×10^{-6}	-34.2
2	1.025	1.047	2.15	0.51	0.51	0.00	2.12×10^{-6}	2.20×10^{-6}	3.77
3	1.100	1.074	-2.36	0.48	0.50	4.17	3.59×10^{-6}	2.93×10^{-6}	-18.4
4	1.071	1.108	3.45	0.50	0.49	-2.00	2.91×10^{-6}	3.00×10^{-6}	3.09
5	1.076	1.101	2.32	0.49	0.50	2.04	2.69×10^{-6}	2.46×10^{-6}	-8.55
6	1.048	1.034	-1.34	0.50	0.50	2.04	2.21×10^{-6}	2.10×10^{-6}	-4.98

Table 11. CrAu/GaN Schottky Contact Clean 2 Measured Device Parameters.

Dev. #	Ideality factor n			SBH ϕ_b (eV)			Leakage Current I_{Leak} (A)		
	Before	After	% diff	Before	After	% diff	Before	After	% diff
1	1.1	1.1	0.00	0.48	0.48	0.00	1.01×10^{-6}	1.13×10^{-6}	11.88
2	1.07	1.07	0.00	0.49	0.49	0.00	1.10×10^{-6}	1.09×10^{-6}	-0.91
3	1.05	1.137	8.29	0.50	0.47	-6.00	3.05×10^{-6}	2.89×10^{-6}	-5.52
4	1.006	1.712	70.2	0.49	0.43	-12.2	1.21×10^{-6}	1.0×10^{-6}	-13.2
5	1.110	1.852	66.9	0.49	0.445	-9.18	9.61×10^{-7}	4.6×10^{-6}	480.8
6	1.112	1.148	3.24	0.47	0.46	-2.13	1.05×10^{-5}	8.38×10^{-6}	-20.3

Table 12. MoAu/GaN Schottky Contact Clean 1 Measured Device Parameters.

Dev. #	Ideality factor n			SBH ϕ_b (eV)			Leakage Current I_{Leak} (A)		
	Before	After	% diff	Before	After	% diff	Before	After	% diff
1	1.09	1.09	0.00	0.56	0.57	1.79	1.95×10^{-7}	1.57×10^{-7}	-19.5
2	1.10	1.15	4.55	0.57	0.58	1.75	5.45×10^{-7}	5.70×10^{-7}	4.59
3	1.09	1.09	0.00	0.585	0.59	0.85	5.05×10^{-7}	5.11×10^{-7}	1.19
4	1.07	1.06	0.93	0.605	0.610	0.83	1.7×10^{-7}	1.74×10^{-7}	1.16
5	1.055	1.045	0.95	0.62	0.63	1.61	1.30×10^{-7}	9.47×10^{-8}	-27.2
6	1.115	1.13	1.35	0.60	0.59	-1.67	2.38×10^{-7}	2.34×10^{-7}	-1.68

Table 13. MoAu/GaN Schottky Contact Clean 2 Measured Device Parameters.

Dev. #	Ideality factor n			SBH ϕ_b (eV)			Leakage Current I_{Leak} (A)		
	Before	After	% diff	Before	After	% diff	Before	After	% diff
1	1.065	1.155	7.79	0.54	0.55	1.85	8.01×10^{-8}	7.92×10^{-8}	-1.14
2	1.04	1.04	0.00	0.495	0.495	0.00	6.12×10^{-8}	6.23×10^{-6}	9902
3	1.09	1.105	1.36	0.52	0.515	-0.96	3.15×10^{-8}	3.24×10^{-5}	9990
4	1.10	1.10	0.00	0.51	0.50	-2.00	4.12×10^{-8}	4.34×10^{-8}	5.07
5	1.06	1.055	-0.47	0.53	0.55	3.77	4.0×10^{-8}	3.54×10^{-8}	-13.0
6	1.08	1.07	-0.93	0.52	0.54	3.85	6.37×10^{-8}	4.79×10^{-8}	-33.0

Table 14. Mo/GaN Schottky Contact Clean 1 Measured Device Parameters.

Dev #	Ideality factor n			SBH ϕ_b (eV)			Leakage Current I_{Leak} (A)		
	Before	After	% diff	Before	After	% diff	Before	After	% diff
1	1.15	1.13	-8.85	0.62	0.59	-5.08	2.38×10^{-8}	3.34×10^{-7}	1402.3
2	1.02	1.02	0.00	0.66	0.66	0.00	1.92×10^{-8}	1.97×10^{-8}	2.54
3	1.02	1.58	54.9	0.65	0.53	-18.5	2.94×10^{-8}	1.97×10^{-5}	6700.0
4	1.16	1.33	14.7	0.62	0.52	-19.2	6.14×10^{-8}	3.72×10^{-6}	6057.0
5	1.03	1.04	0.97	0.66	0.66	0.00	2.36×10^{-8}	3.67×10^{-8}	54.25
6	1.03	1.02	-0.97	0.62	0.66	6.45	4.66×10^{-8}	5.02×10^{-8}	7.17

Table 15. Mo/GaN Schottky Contact Clean 2 Measured Device Parameters.

Dev. #	Ideality factor, n			SBH, ϕ_b (eV)			Leakage Current I_{Leak} (A)		
	Before	After	% diff	Before	After	% diff	Before	After	% diff
1	1.14	1.05	-7.89	0.55	0.57	3.64	4.21×10^{-6}	6.23×10^{-5}	1479.0
2	1.03	1.03	0.00	0.50	0.60	20.0	2.90×10^{-8}	3.71×10^{-8}	27.93
3	1.00	1.02	2.00	0.63	0.625	0.79	1.96×10^{-8}	1.92×10^{-8}	-2.04
4	1.00	1.02	2.00	0.65	0.64	1.54	1.73×10^{-8}	1.63×10^{-8}	-5.78
5	1.01	1.035	2.48	0.65	0.63	3.08	1.20×10^{-8}	1.06×10^{-8}	-11.7
6	1.00	1.01	1.00	0.65	0.63	3.08	1.3×10^{-8}	1.59×10^{-8}	22.3

LIST OF REFERENCES

[1] U.S. Department of Energy. (September 2015). *Quadrennial technology review 201.5* Washington, DC. [Online]. Available: http://energy.gov/sites/prod/files/2016/02/f29/QTR2015-6N-Wide-Bandgap-Semiconductors-for-Power-Electronics.pdf

[2] M. A. Khan, R. A. Skogman, R. G. Schulze, and M. Gershenzon, "Electrical properties and ion implantation of epitaxial GaN, grown by low pressure metalorganic chemical vapor deposition," *Appl. Phys. Lett.*, vol. 42, no. 5, pp. 430–431, Mar., 1982.

[3] A. C. Schmitz, A. T. Ping, M. A. Khan, Q. Chen, J. W. Yang, and I. Adesida, "Schottky barrier properties of various metals on n-type GaN," *Semicond. Sci. Technol.*, vol. 11, pp. 1464–1467, July 1996.

[4] S. M. Sze and C. R. Crowell, "Current transport in metal-semiconductor barriers," *Solid-State Electron.*, vol. 9, no. 11–12, pp. 1035–1048, 1966.

[5] L. Wang, M. I. Nathan, T-H. Lim, M. A. Khan, and Q. Chen, "High barrier height GaN Schottky diodes: Pt/GaN and Pd/GaN," *Appl. Phys. Lett*., vol. 68, no. 9, pp. 1267–1269, Feb., 1996.

[6] X. Zhang, "Failure mechanisms in wideband semiconductor power devices," Ph.D. dissertation, Dept. Elect. and Comp. Eng., Univ. of Maryland, College Park, 2006.

[7] S. Yoshimoto, M. Okada, F. Mitsuhashi, T. Ishizuka, and M. Ueno, "Fast recovery performance of vertical Schottky barrier diodes on low dislocation density freestanding GaN substrates," *SEI Tech. Rev.*, no. 80, pp. 35–39, Apr., 2015.

[8] S. O. Kasap, "Semiconductors," in *Principles of Electronic Materials and Devices*, 3rd ed. New York: McGraw-Hill, 2006, pp. 435–443.

[9] B. G. Streeman, "Junctions," in *Solid State Electronic Devices,* 4th ed. New Jersey: P.H., 1997, pp. 183–190.

[10] S. M. Sze and K. K. Ng, "Metal-semiconductor contacts," in *Physics of Semiconductor Devices,* 3rd ed. New Jersey: Wiley, 2007, pp. 134–196.

[11] B. V. Zeghbroeck, "Metal-semiconductor fundamentals," in *Principles of Semiconductor Devices*, 1st ed. [Online]. Available: http://ecee.colorado.edu/~bart/book/book/title.htm

[12] R. T. Tung, "The physics and chemistry of the Schottky barrier height," *Appl. Phys. Rev.*, vol. 1, no. 1, pp 1–53,Mar. 2014. [Online]. Available: http://scitation.aip.org/content/aip/journal/apr2/1/1/10.1063/1.4858400

[13] R. T. Tung. (2014) *Electrostatic Potential: The Key to Band Alignment Problems* [Online]. http://academic.brooklyn.cuny.edu/physics/tung/Schottky/potential.htm

[14] J. Bardeen, "Surface sates and rectification at a metal semi-conductor contact," *Phys. Rev.*, vol. 71, no. 10, pp. 717, May, 1947.

[15] V. Heine, "Theory of surface states," *Phys. Rev.*, vol. 138, no., 6A, pp. A1689-A1696, June, 1965.

[16] R. T. Tung, "Formation of an electric diploe at metal-semiconductor interfaces," *Phys. Rev. B*, vol. 64, no. 20, pp. 1–10, Nov., 2001.

[17] R. Balsano, C. Durcan, A. Matsubayashi, A. Narasimham, and V. LaBella, "Relating spatially resolved maps of Schottky barrier height to metal/ semiconductor interface composition," *J. Appl. Phys.*, Vol. 119, no. 9, Mar., 2016.

[18] R. T. Tung, "Electron transport at metal-semiconductor interfaces: general theory," *Phy. Rev.*, vol. 45, no. 23, pp. 13509-13522, June, 1992.

[19] J. H. Werner, and H. H. Guttler, "Barrier inhomogeneities at Schottky contacts," *J. Appl. Phys.*, vol. 69, no. 3, pp. 1522–1533, Feb., 1991.

[20] K. Sarpatwari, "Toward understanding the electrical properties of metal/ semiconductor Schottky contacts: the effect of barrier inhomogeneities and geometry in bulk and nanosacle structures," Ph.D. dissertation, Dept. Eng. Sci. and Mech., Penn. State Univ., State College, 2009.

[21] F. A. Padovani, and G. G. Sumner, "Experimental study of gold-gallium arsenide Schottky barriers," *j. Appl. Phys.*, vol. 36, no. 12, pp. 3744–3747, Apr., 1965.

[22] A. Kumar, S. Arafin, M. Amann, and R. Singh, "Temperature dependence of electrical characteristics of Pt/GaN Schottky diode fabricated by UHV e-beam evaporation," *Nanoscale Res. Lett.*, vol. 8, no. 1, pp. 1–7, Nov., 2013.

[23] K. Chen, H. Lin, S. Cheng, Y. Peng, G. Shen, L. Chen, C. Chen, J. Huang, and K. Tu, "Silicide formation in implanted channels and interfacial reactions of metal contacts under high current density," *J. Mater. Res.*, vol. 14, no. 12, pp. 4720–4726, Dec., 1999.

[24] T. Horiuchi, and Y. Sugawara, "Long-term reliability of evaluation of power semiconductor devices used in substation rectifiers," in *Proc. International Symposium Power Semiconductor Devices & Integrated Circuits,* Kyoto, 1998, pp. 195–198.

[25] J. Huang, K. Tu, S. Bedell, W. Lanford, S. Cheng, J. Lai, and L. Chen, "Polarity effect on failure of Ni and Ni_2 Si contacts on Si," *J. Appl. Phys.*, vol. 82, no. 5, pp. 2370–2377, Sept., 1997.

[26] M. Brandt, V. Krozer, M. Schubler, K. Bock, and H. Hartnagel, "Characterization of reliability of compound semiconductor devices using electrical pulses," *Microelectron. Reliab.*, vol. 36, no. 11/12, pp. 1891–1894, 1996.

[27] B. Downey, J. Flemish, B. Liu, T. Clark, and S. Mohney, "Current-induced degradation of nickel ohmic contacts to SiC," *J. Electron. Mater.*, vol. 38, no. 4, pp. 563–568, Apr., 2009.

[28] B. Downey, S. Mohney, T. Clark, and J. Flemish, "Reliability of aluminum-bearing ohmic contacts to SiC under high current density," *Microelectron. Reliab.*, vol. 50, no. 12, pp. 1967–1972, Dec., 2010.

[29] E. Zanoni, M. Meneghini, A. Chini, D. Marcon, and G. Meneghesso, "AlGaN/ GaN-based HEMTs failure physics and reliability: mechanisms affecting gate edge and Schottky junction," *IEEE Trans. Electron Devices*, vol. 60, no. 10, pp. 3119–3131, Oct., 2013.

[30] R. Lin, I. Mehdi, A. Pease, R. Dengler, D. Humphrey, T. Lee, A. Scherer, and S. Kayali, "Accelerated lifetime testing and failure analysis of quartz based GaAs planar Schottky diodes," in *Proc. GaAs Reliability Workshop*, Anaheim, CA, 1997, pp. 19–39.

[31] D. Cheney, E. Douglas, L. Liu, C. Lo, B. Gila, F. Ren, and S. Pearton, "Degradation mechanisms for GaN and GaAs high speed transistors," *Mater.*, vol. 5, no. 12, pp. 2498–2520, Nov., 2012.

[32] Gallium nitride: basic parameters for Wurtzite crystal structure (n.d.). Ioffe Physico-Technical Institute. [Online]. http://www.ioffe.ru/SVA/NSM/Semicond/ GaN/basic.html. Accessed Aug. 17, 2016.

[33] R. Tompkins, M. Khan, R. Green, K. Jones, and J. Leach, "IVT measurements of GaN power Schottky didoes with drift layers grown by HVPE on HVPE GaN substrates," *J. Mater. Sci. – Mater. Electron.*, vol. 27, no. 6, pp. 6108–6114, June 2016.

[34] M. Missous, and E. Rhoderick, "On the Richardson constant for aluminum/ gallium arsenide Schottky diodes," *J. Appl. Phys.*, vol. 69, no. 10, pp. 7142–7145, May, 1991.

THIS PAGE INTENTIONALLY LEFT BLANK

INITIAL DISTRIBUTION LIST

1. Defense Technical Information Center
   Ft. Belvoir, Virginia

2. Dudley Knox Library
   Naval Postgraduate School
   Monterey, California